

# Surfactant Directed Encapsulation of Metal Nanocrystals in Metal-Organic Frameworks

Author: Pan Hu

Persistent link: <http://hdl.handle.net/2345/bc-ir:104132>

This work is posted on [eScholarship@BC](#),  
Boston College University Libraries.

---

Boston College Electronic Thesis or Dissertation, 2015

Copyright is held by the author. This work is licensed under a Creative Commons Attribution 4.0 International License. <http://creativecommons.org/licenses/by/4.0/>

Boston College  
The Graduate School of Arts and Sciences  
Department of Chemistry

SURFACTANT DIRECTED  
ENCAPSULATION OF METAL  
NANOCRYSTALS IN METAL-ORGANIC  
FRAMEWORKS

A thesis by

PAN HU

Submitted in partial fulfillment of the requirements  
for the degree of

Master of Science

May 2015

© copyright by PAN HU

2015

# Surfactant Directed Encapsulation of Metal Nanocrystals in Metal-Organic Frameworks

Pan Hu

Advisor: Prof. Chia-Kuang Tsung

## **Abstract**

Metal nanocrystals with size and shape control have great potential in heterogeneous catalysis. Controllable encapsulation of well-defined metal nanoparticles into the novel porous materials results in new multifunctional nanomaterials. The core-shell nanostructure can enhance the selectivity, durability, or reactivity of the catalysts and even provide additional functionalities. Metal-organic frameworks (MOFs) are a class of novel crystalline nanoporous materials, with well-defined pore structures and distinctive chemical properties. Using MOFs as the encapsulating porous materials has drawn great interest recently due to their tunable structures and properties. However, it could be challenging to grow another porous material layer on metal surface due to the unfavorable interfacial energy. In this work we develop a new concept of colloidal synthesis to synthesize the metal@MOF core-shell nanostructures, in which a layer of self-assembled molecules directed the growth and alignment between two materials.

Surfactant cetyltrimethylammonium bromide (CTAB) is designated to facilitate the overgrowth of MOF onto metal surface, and an alignment between the  $\{100\}$  planes of the metal and  $\{110\}$  planes of the MOF can be observed. By utilizing the same concept, a third layer of mesoporous silica could also be coated on the MOF shell with assistance of CTAB. And our method could be a general strategy to fabricate multiple-layer MOF materials.

## Keywords

Metal Nanocrystal, Metal-Organic Frameworks, Core-Shell Structure, Catalysis

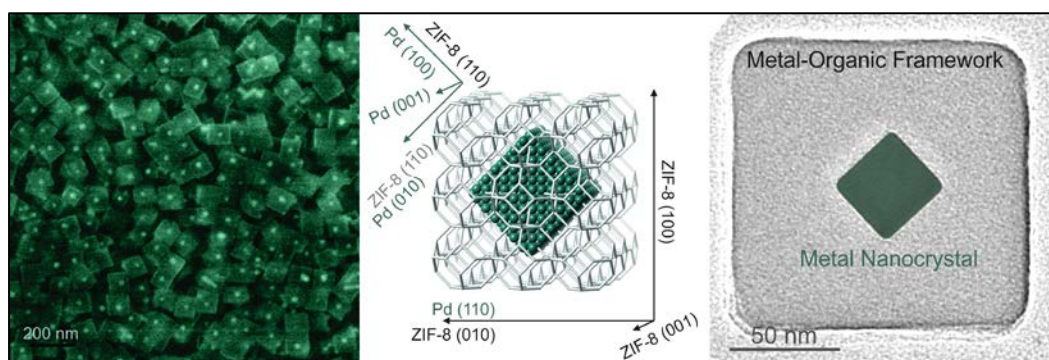


# Table of Contents

<b>Chapter 1: Introduction</b> .....	1
1.1 Metal@Porous Material Core-Shell Structures.....	1
1.2 Advantage of Metal-Organic Frameworks as Shell .....	3
1.3 General Approach to Synthesize Metal@MOF Core-Shell Nanoparticles .....	5
1.3.1 “Ship-In-a-Bottle” approach .....	6
1.3.2 “Bottle-around-Ship” or <i>de novo</i> approach.....	8
1.4 Research Motivation .....	9
<b>Chapter 2: Experimental Part</b> .....	13
Chemicals and Materials.....	13
Instrumentation .....	13
2.1 Room Temperature Synthesis of Cubic ZIF-8 Nanoparticles in Aqueous Condition.....	15
2.2 Synthesis of Various Types of Noble Metal Nanoparticles .....	16
2.3 Encapsulation of metal nanocrystals into ZIF-8 cube .....	17
2.4 Coating of mesostructured silica layer.....	19
2.5 Overgrowth of MOF on pure MOF, and metal@MOF particles.....	19
<b>Chapter 3: Characterization and Analysis</b> .....	20
3.1 Structures and Compositions of metal@MOF core-shell nanocrystals.....	21
3.2 Alignments between metal core and MOF.....	29
3.3 Catalytic Applications in alkene hydrogenation.....	33

<b>Chapter 4: Discussion</b> .....	36
4.1 Growth Mechanism of Metal@ZIF-8 .....	36
4.2 Role of Surfactant in the Overgrowth of ZIF-8 on Metal .....	38
4.3 General strategy to synthesize multiple-layer core-shell/yolk-shell MOF nanostructures.....	41
<b>Chapter 5: Conclusion</b> .....	44

## List of Figures

<b>Figure 1.</b> Various types of core-shell structures.....	3
<b>Figure 2.</b> Formation of nanocrystals encased individually and aligned in single-crystalline porous materials. ....	12
<b>Figure 3.</b> Overview of the synthesis of metal nanoparticles, cubic ZIF-8 particles, and Pd/Au@ZIF-8 core-shell nanoparticles.....	15
<b>Figure 4.</b> Scheme illustrates the encapsulation of Pd/Au nanoparticles into cubic ZIF-8. ....	18
<b>Figure 5.</b> TEM images of Pd nanocube (A); Au octahedron (B); ZIF-8 nanocube (C, D). SEM images of ZIF-8 with particle size from 150 nm to 60 nm (E, F, G). ....	22
<b>Figure 6.</b> (A) SEM and (B) TEM images of Pd@ZIF-8 core-shell nanostructures. ....	23
<b>Figure 7.</b> TEM images of Pd@ZIF-8 with different average shell thicknesses: 60 nm (A, B); 35 nm (C, D).....	24
<b>Figure 8.</b> Powder XRD pattern of Au@ZIF-8 and Pd@ZIF-8. ....	25
<b>Figure 9.</b> TEM images of mesoporous SiO <sub>2</sub> synthesis without Pd nanocubes, before acid treatment (A), and after acid treatment (B, C).....	27
<b>Figure 10.</b> TEM images of (A, B) Pd@ZIF-8@mSiO <sub>2</sub> with alignment from atomic to mesoscopic scales and (C) Pd@mSiO <sub>2</sub> yolk-shell nanocomposite with cylindrical mesostructured channels.....	27
<b>Figure 11.</b> SAXS/PXRD of Pd@ZIF-8@mSiO <sub>2</sub> . ....	28
<b>Figure 12.</b> TEM images of mSiO <sub>2</sub> synthesis without CTAB. No coating on ZIF-8 was observed, and only formed small silica nanoparticles could be seen on the background. ....	29

<b>Figure 13.</b> TEM images of Pd@ZIF-8 (A, D). Perspective view of the 3D models (B, E). Projections of the 3D modelling that match the TEM image well (C, F).....	30
<b>Figure 14.</b> TEM images and corresponding 3D modelling of Au@ZIF-8 core-shell nanoparticles. [100] view of TEM images and projection (A, B, F), [010] view of TEM images and projection (C, D, G). Perspective view (E).....	31
<b>Figure 15.</b> TEM image (A, B) and 3D modeling of Pd {100} aligned with ZIF-8 {100} (perspective: C, projection: D).....	32
<b>Figure 16.</b> Illustration of size selective alkene hydrogenation reaction catalyzed by Pd@ZIF-8 core-shell nanoparticles.....	34
<b>Figure 17.</b> TEM images of Au@ZIF-8 (A, B, C) and Pd@ZIF-8 (D, E, F) that were arrested at early stage of the reaction.....	38
<b>Figure 18.</b> SEM images (A), Raman shift (B), and SERS intensity of four reaction stages.....	39
<b>Figure 19.</b> TEM images of Au octahedron@ZIF-8 with polycrystalline shell (A: Low magnification, B: a single Au@ZIF-8 particle).....	40
<b>Figure 20.</b> SEM images of ZIF-67 (A, B). Picture of the reaction solution shows the bright purple color of this Cobalt containing MOF (C). .....	41
<b>Figure 21.</b> SEM images of ZIF-8@ZIF-8, ZIF-8@ZIF-8@ZIF-8 (A, B). TEM images of ZIF-8@ZIF-67 (C, D) and ZIF-67@ZIF-8 (E, F). .....	42
<b>Figure 22.</b> TEM images of Pd @ZIF-8@ZIF-8 (A), Au@ZIF-8@ZIF-8 (B), ZIF-8@ZIF-8 yolk-shell/core-shell nanoparticles (C, D).....	43

## List of Tables

<b>Table 1.</b> Elemental analysis by ICP-OES. The loading amount of metal in ZIF-8 was relatively high. No significant loss of metal nanoparticles during the ZIF-8 coating was observed.....	26
<b>Table 2.</b> Particle size distribution and mis-oriented particle percentage.....	33
<b>Table 3.</b> Heterogeneous catalysis for Pd@ZIF-8 and Pd on ZIF-8 support: hydrogenation of ethylene and cyclooctene, activity and activation energy.....	35

## List of Abbreviation:

MOF	Metal-Organic Framework
ZIF-8	Zeolitic Imidazolate Framework-8
CTAB	Cetyltrimethylammonium Bromide
PVP	Polyvinylpyrrolidone
SEM	Scanning Electron Microscope
TEM	Transmission Electron Microscopy
PXRD	Powder X-Ray Diffraction

## Chapter 1: Introduction

Heterogeneous catalysts can change the pathway of chemical reaction, lower the activation energy and thus increase the reaction rate, which endows the catalysts with a wide range of applications in many industrial processes, such as chemical manufacturing, oil refining, energy conversion, and pollution treatment.<sup>1, 2</sup> Metal particles with sizes in the nanoscale, especially the noble metal nanocrystals with various structures and compositions, are well-studied as the novel high-efficient heterogeneous catalysts due to their high surface-to-volume ratio and high percentage of undercoordinated surface atoms. They also exhibit unique optical, electrical, and magnetic properties that differ from bulk materials. The reactant molecules are absorbed on the metal surface and undergo the catalytic reactions. Recent progresses in nanotechnology and colloidal chemistry enable people to rationally engineer the sizes, shapes, facets, defects, and chemical compositions of metal nanoparticles, thus the catalytic properties such as activity and selectivity could also be properly tuned.

3-29

### 1.1 Metal@Porous Material Core-Shell Structures

A new approach to enhance the catalytic performances of metal nanoparticles is to fabricate the nanoscale catalyst into core-shell structures.<sup>30-47</sup> Metal nanoparticles tend to aggregate together or sinter into each other to reduce the overall surface energy

under the reaction conditions, usually high temperature and pressure. This restructure deforms the particle morphology, decreases the surface area and very often lowers the activity or selectivity of the catalyst. By encapsulating well-defined metal nanocrystal core into porous material shell, we can maintain or enhance the activities of metal catalysts, as well as imparting more functionalities to the composite. The porous shell ensure the accessibility of reactant molecules to the active metal surface, meanwhile it provides several advantageous improvements. For example, the porous shell can increase the durability of the catalysts against the harsh conditions, introduce size selectivity towards different reactant molecules, tune the diffusion rate, enrich the reactant molecules, and manipulate the orientation or configuration of the molecules absorbed on the surface.

The metal@porous material core-shell structured catalysts can be categorized into different types based on their structural characteristics.<sup>42-44, 46, 48-52</sup> Here we demonstrate some of the frequently reported core-shell structures in Figure 1: (a) one metal core coated by a layer of porous shell; (b) multiple cores encapsulated in a matrix porous material particle; (c) “yolk-shell” or “bell” structures, consisting of a core encased in a hollow shell with a void/cavity in between.

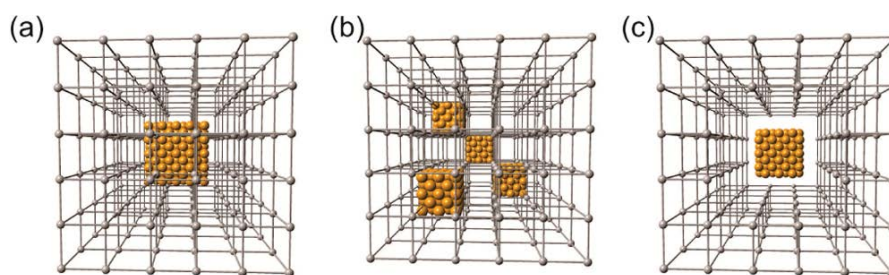


**Figure 1.** Various types of core-shell structures. (A) single core-shell structure; (B) multiple cores in one shell structure; (C) yolk-shell structure. Copyright © American Chemical Society 2014.

Various types of metal@porous material core-shell nanostructures have been successfully synthesized, with different porous materials as shell, such as silica,<sup>32, 37, 42, 48-50</sup> carbon,<sup>33, 34, 36, 51</sup> metal oxides,<sup>31, 52-57</sup> and polymers.<sup>47, 58</sup> Somorjai and co-workers<sup>37</sup> reported Pt@mesoporous SiO<sub>2</sub> core-shell structures that have excellent thermal stability at high temperature. Dai,<sup>59</sup> Matsumura,<sup>36</sup> and co-workers showed examples of Pt and Au nanoclusters encapsulated into porous carbon, and the catalysts exhibit activity in hydrogenation and reduction. Metal nanoparticles incorporated in metal oxide shells have also been applied as core-shell structured nanocatalysts.<sup>52-54, 60-62</sup> The success in enhancement of the catalytic performances in core-shell structures has inspired people to extend the range of shell materials and search for better novel porous materials.

## 1.2 Advantage of Metal-Organic Frameworks as Shell

Metal-organic frameworks (MOFs), also known as porous coordination polymers (PCPs), are a class of emerging crystalline nanoporous materials with tunable structures and unique properties.<sup>63-91</sup> The MOF consists of two main components: bridging organic linkers and inorganic secondary building units (SBUs) such as metal ions or metal oxide clusters. The organic linkers are ditopic or polytopic organic molecules with negative charges, which can strongly bind to metal containing SBU, to generate architecturally stable highly crystalline structures with permanent open porosity. The chemical compositions and topological structures of metal-organic frameworks can be vastly varied with over 20,000 different MOFs being reported in the past years. Compared to traditional inorganic nanoporous material such as zeolite, MOF has several advantages such as ultrahigh porosity and internal surface area, tunable pore size, adjustable internal surface, and modifiable organic linkers. These features endow MOF with a wide range of potential applications, such as gas storage and separation,<sup>92-95</sup> molecular sensing,<sup>96-98</sup> drug delivery,<sup>99-101</sup> host-guest chemistry,<sup>72</sup> and heterogeneous catalysis.<sup>69, 71, 75</sup> A lot of efforts have been put in the exploration of new MOF structures and various applications, even leading to commercialization of some types of MOF.<sup>102</sup> It is desirable to further exploit the unique properties of this novel nanoporous material. Combination of MOF with other functional materials for composite materials with sophisticated structures has been proposed recently as an effective way to achieve property synergies for multifunctional applications. Many functional materials can be integrated with MOFs, including metal oxides, quantum dots (QDs), polyoxometalates (POMs), polymers, carbon nanostructures,

biomolecules,<sup>103</sup> and metal nanoparticles.<sup>91, 104-116</sup> The composite materials of MOF and other species allow new chemistry that cannot be realized through one-component materials. Among these, encapsulation of metal nanoparticles into MOF has been extensively investigated, especially for the applications of catalysis. Compared with other porous materials, MOF as a shell material offers several advantages for catalysis: (i) the well-defined nanoporosity in MOF impart confinement effects and shape selectivity to the composite catalyst; (ii) appropriate organic linkers of MOF shell can provide interaction with metal nanoparticle core; (iii) the great diversity and abundance of MOF structures enables the easy selection of a proper MOF as the host matrix; (iv) milder synthetic conditions maintain the morphologies and functionalities of metal nanoparticles.

### **1.3 General Approach to Synthesize Metal@MOF Core-Shell Nanoparticles**

The methodologies for encapsulation of nanoparticles into MOF focus on two main directions. The first and widely used one is known as “ship-in-a-bottle” approach, which involves the introduction of metal precursors (gas-phase or liquid-phase) into the pre-synthesized MOF matrix, and then reduction or decomposition of the precursors, thus metal particles were deposited within the cavities of MOF. This approach is straightforward with less complicated interface and interaction between metal core and MOF shell. The pores of the MOFs are used as template to confine the

growth of the nanoparticles to a small size (usually less than 5 nm). The overall structure and morphology of the MOF maintained throughout the whole process, however to control the size, shape, and composition of metal nanocrystals is challenging. In addition, particles formed inside the framework could block the pores thus lower the surface area of MOF; also the metal precursors or reduction products may diffuse out through the pores and form particles undesirably on the external surface of MOF. The second one is known as “bottle-around-ship” approach, or *de novo* synthesis, which involves the controlled assembly of MOF precursors around the pre-synthesized metal nanoparticles. By this method, all the intrinsic properties of nanoparticles such as size, shape, and composition can be fully preserved after MOF coating due to the relatively mild condition. Nevertheless, the controlled overgrowth of MOF shell on metal nanoparticle core rather than self-nucleation is challenging, due to the large interfacial energy barrier between the two materials with crystal lattices in different scales. Besides, capping agents absorbed on the nanoparticle surface are necessary for successful coating of MOF shell, which results in a more complicated interface between the MOF and the metal, and sometimes may hinder the catalysis of the metal core.

### **1.3.1 “Ship-In-a-Bottle” approach**

Similar to the traditional synthesis of metal@zeolite composite, gas-phase infiltration, liquid-phase impregnation, and solid-state grinding methods are first adopted by the

researchers to deposit metal nanocrystal into cavities of MOF. Fischer and co-workers<sup>117-122</sup> choose gas-phase organometallics as metal precursors, which can be reduced and decomposed to generate metal particles. This is an efficient way to deposit metal nanocrystals within the MOF by chemical vapor deposition (CVD). In a typical synthesis, the chosen MOF matrix is exposed to the vapor of gaseous organometallic precursors in sealed Schlenk tube. The volatile precursors diffuse into the nanopores of MOF, then either hydrogen is added to reduce the organometallics, or temperature is increased to thermally decompose the precursors, therefore metal nanoparticles formed in the nanopores of MOF and the size is confined by the pore size. Due to the limitations of water/air-sensitive gas phase organometallic precursors, Xu and co-workers<sup>123-127</sup> developed the liquid-phase impregnation method, which metal salt solution was reduced to metal particles in the cavities of MOF. Typically, a MOF support is soaked in the solution containing the metal precursors, usually in the form of chloride or nitrate salts. The metal ions infiltrated into the empty pores by capillary force, followed by the reduction of metal precursor by hydrogen gas or sodium borohydride, to yield the deposited metal within the nanopores of MOF. They also developed a double solvent method (DSM) to reduce the chances of metal particle aggregation on the external surface of MOF. This method is a combination of the aqueous solution contains metal precursors and large amount of organic solvent that can improve the dispersion of absorbent and facilitate the impregnation process. The small amount of precursor solution was pushed inside the hydrophilic pore, thus minimizing the deposition of metal on external surface. The “ship-in-a-bottle”

approach is an efficient way to produce ultra-small metal nanocrystals in MOF. However, the controllable composition and shape of metal core is highly desired in some applications, which is lack in this method. In addition, the locations of metal particles in the MOF matrix are often randomly distributed, and loading amount is also limited. Different strategy is needed to overcome such disadvantages and lead to better utilization.

### **1.3.2 “Bottle-around-Ship” or *de novo* approach**

Recently, a new synthetic strategy, called “bottle-around-ship” or *de novo* approach is developed, in which the pre-synthesized metal nanocrystals are introduced into the solution containing MOF precursors. During the nucleation and growth of MOF crystals, the metal nanoparticles are subsequently integrated into the MOF matrix. The size, shape, chemical composition, and intrinsic properties of the metal core are fully preserved after the coating of MOF shell. Compared to the “ship-in-a-bottle” strategy, this method provides more opportunities in catalytic or optical applications, due to the better control of shapes, compositions of both metal core and MOF shell, as well as the interface in between. Sada and co-workers<sup>128, 129</sup> report the first example of Au nanorod-MOF composite using this new strategy. The Au nanorods are first synthesized by a seed mediated method in water, then added into the *N,N*-diethylformamide (DEF) solutions containing MOF precursors. The Au@MOF was successfully fabricated by the direct growth of MOF on the surface of Au

nanorods. Hupp, Huo and co-workers<sup>130, 131</sup> incorporated various polyvinylpyrrolidone (PVP) capped nanoparticles into zeolitic imidazolate framework-8 (ZIF-8, a type of MOFs) crystal, including noble metal nanocrystals, magnetic nanoparticles, quantum dots, and up-conversion nanoparticles. The pre-formed PVP capped nanoparticles are introduced into the methanolic solution of ZIF-8 precursors, 2-methylimidazole and zinc nitrate at room temperature, and thus the particles are encapsulated into the ZIF-8, through the adsorption of metal particles on the continuously forming fresh surfaces of growing MOF sphere. The introduction of amphiphilic surfactant PVP into the synthetic solution is crucial to the successful encapsulation, which can increase the stability of the nanoparticle in polar solvent, such as methanol, *N,N*-dimethylformamide (DMF) that are commonly used in MOF synthesis, and enhance the interaction between nanoparticles and metal-organic frameworks. Compared with the “ship-in-a-bottle” method in which metal precursors were deposited into MOF matrix, the *de novo* synthesis by assembling the MOF precursors around metal nanocrystals has several significant advantages. For instance, the size of metal nanoparticle is no longer limited by the pore size of MOF; a variety of sizes, shapes, and compositions of metal core can be achieved by the well-developed synthetic methods; active properties of metal nanoparticles can be properly preserved after MOF coating; the spatial distribution of embedded metal core within MOF support shell can be controlled only in “bottle-around-ship” approach.

## **1.4 Research Motivation**

Interface between two different materials is important for catalysis. Fundamental understanding and rational engineering of interface between the metal catalyst core and nanoporous material shell will be crucial to the catalytic activity because the structure at the interface could change the sorption behaviors of reactant molecules on the catalyst surface, which significantly affects the yield and selectivity of the product. Careful examination of the binding, transformation and transportation of interface species between two domains is necessary when designing a new composite catalyst or improving the catalytic performance. A controlled alignment at the interface between materials across a wide range of size scales is critical to composite materials, especially for composite nanomaterials as their interfaces exist in the mesoscale, where classical physics, quantum mechanics, and nanoscience meet. Few previous reports show a good control of alignment or interfacial design for metal@MOF core-shell nanocatalyst.

Many factors need to be carefully considered and optimized for a successful encapsulation, including the interactions between the MOF shell and metal core, the capping agents absorbed on particle surface, the interface between two different materials, the compatibility of the nanoparticles, and the MOF synthesis conditions. Among these, a proper interaction between the MOF and nanoparticle surface is the critical parameter of “bottle-around-ship” approach, because MOF tend to self-nucleate and form individual particles rather than overgrow on the metal particles.

Capping agents are widely utilized to prevent the nanoparticles from aggregation or sintering in solution, as well as to promote the MOF overgrowth on metal surface, because surface energy barriers can be significantly lowered by the surfactants. Meanwhile, the capping agent may result in more complicated interfaces between the MOF and metal surface. It may negatively affect the catalytic performance if the capping agent on the metal surface cannot be effectively removed after the MOF coating. Previous works have shown that the addition of polymer molecules such as PVP could promote the overgrowth of MOF; however, due to the polymer nature of polymer molecules, controlled alignment between core and shell had not been observed. The structure control in most of these studies is also not optimized yet. Either multiple metal particles are encased in one giant MOF crystal with random orientations, or one metal nanocrystal is surrounded by a polycrystalline MOF shell. The shell composed by granular MOF crystals may have defects or cracks that unfavorable for catalytic applications. The structure of nanoparticles individually encased in single crystalline MOF crystals in a one-to-one structure has not been achieved, to say nothing of a controlled alignment between the lattices of nanoparticles and MOFs.

In this work, we utilize ionic surfactant molecules, cetyltrimethylammonium bromide (CTAB), to bridge the noble metal (palladium and gold) and zeolitic imidazolate framework-8 (ZIF-8) surfaces, as well as to facilitate the controlled alignment between the core and shell. The metal@MOF core-shell nanocomposites synthesized here are

composed of single well-defined metal nanocrystals individually encased in ZIF-8 nanocrystals, and we proposed a formation mechanism for metal@ZIF-8 core-shell structures (Figure 2). Highly ordered self-assembled alkanethiol molecular layers have been proved to align the overgrowth of MOF on metal thin films in the self-assembled monolayer (SAM) system. Similarly we adopt this concept in our colloidal system, but instead surfactant CTAB molecules are chosen to form the self-assembled layered structures on the surface of metal nanocrystals in aqueous solutions. The molecular layer of CTAB can intermediate the interaction between metals and ZIF-8, as well as stabilize specific facets of the metals and MOFs, so an alignment between the crystal structures of the cores and shells is expected. This colloidal synthesis is further applied to fabricate MOF nanostructures with multiple layer, including core-shell, yolk-shell MOF@MOF nanocrystals.

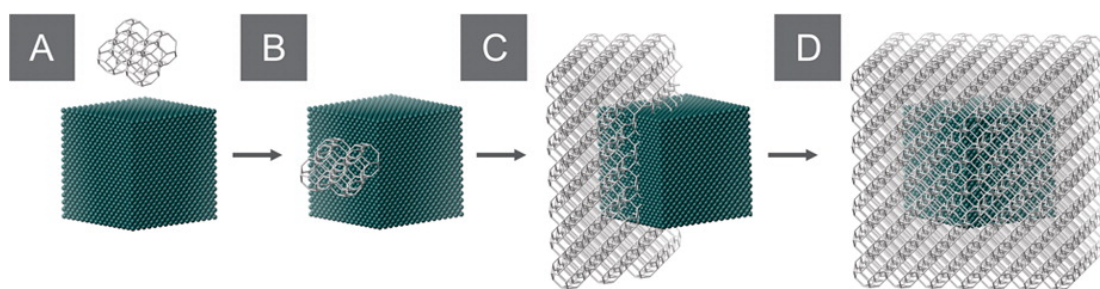


**Figure 2.** Formation of nanocrystals encased individually and aligned in single-crystalline porous materials. (A) Introduction of well-defined nanocrystals after the nucleation of ZIF-8. (B) Single crystalline ZIF-8 nucleus attachment to the metal surface with selective orientation. (C) ZIF-8 crystal growth on the nucleus. (D) Single nanocrystal captured in single crystalline ZIF-8 with lattice alignment. Copyright © American Chemical Society

2014.

## Chapter 2: Experimental Part

### Chemicals and Materials

Cetyltrimethylammonium bromide (CTAB, CalBioChem, 98%), ascorbic acid (Sigma-Aldrich, 99%), hydrogen tetrachloroaurate trihydrate ( $\text{HAuCl}_4 \cdot 3\text{H}_2\text{O}$ , Sigma-Aldrich, ~50% Au basis), hydrogen tetrachloropalladate ( $\text{H}_2\text{PdCl}_4$ , Sigma-Aldrich, 98%), zinc nitrate hexahydrate ( $\text{Zn}(\text{NO}_3)_2 \cdot 6\text{H}_2\text{O}$ , Sigma-Aldrich, 99%), cobalt nitrate hexahydrate ( $\text{Co}(\text{NO}_3)_2 \cdot 6\text{H}_2\text{O}$ , Sigma-Aldrich, 99%), 2-methylimidazole (Sigma-Aldrich, 99%), polyvinylpyrrolidone (PVP, M.W. ~29000, Sigma-Aldrich), sodium bromide (NaBr, Sigma-Aldrich, 99%), sodium borohydride ( $\text{NaBH}_4$ , Sigma-Aldrich, 99%), ethylene (Airgas, 99.995%), *cis*-cyclooctene (Sigma-Aldrich, 95%), sodium hydroxide (NaOH, Sigma-Aldrich, 98%), tetraethyl orthosilicate (TEOS, Sigma-Aldrich, 98%) were used without further purification. Ultrapure deionized water (d. i.  $\text{H}_2\text{O}$ , 18.2 M $\Omega$ ) was used for all solution preparations. Hydrogen ( $\text{H}_2$ , Airgas, 99.999%) and helium (He, Airgas, 99.999%) were used for heterogeneous catalysis.

### Instrumentation

Transmission electron microscopy (TEM), including high resolution transmission electron microscopy (HR-TEM) was performed on a JEOL JEM2010F electron microscope operated at 200 kV. Samples for TEM were prepared by diluting 50  $\mu\text{L}$  sample solution to 500  $\mu\text{L}$  and placing 2.0  $\mu\text{L}$  droplets onto carbon-coated copper grids, then allowed to dry under a heat lamp. Normal scanning electron microscopy (SEM) was performed on a JEOL JSM6340F scanning electron microscope. Samples were prepared for SEM by diluting 50  $\mu\text{L}$  sample solution to 500  $\mu\text{L}$  and placing a 1.0  $\mu\text{L}$  droplet onto silicon wafer and drying under a heat lamp. The samples were then placed on silver glue atop double-sided copper tape on sample holder. Powder X-ray diffraction (PXRD) patterns were collected on a Bruker D2 diffractometer. Samples for XRD were prepared by drying the sample solution in an oven and scraping the sample powder onto a sample holder. Small-angle X-ray scattering (SAXS) was performed under beamline BL01C2 (beam energy 18 keV) in National Synchrotron Radiation Research Center (NSRRC), Taiwan. Surface-enhanced Raman spectroscopy (SERS) was performed using x-y imaging mode of a Nanophoton Ramantouch microspectrometer with an excitation wavelength of 785 nm. A 100 $\times$  (N.A. 0.9) objective lens with 60 s accumulation time was used for data collection between 455  $\text{cm}^{-1}$  to 1583  $\text{cm}^{-1}$ . For the following SEM studies with SERS, a JEOL JSM7600F microscope was used. Samples for ICP-OES were prepared by dissolving oven dry powders in 5% nitric acid, and diluting to proper concentrations. ICP-OES was performed on a Perkin Elmer optima 2100DV ICP-OEX spectrometer.

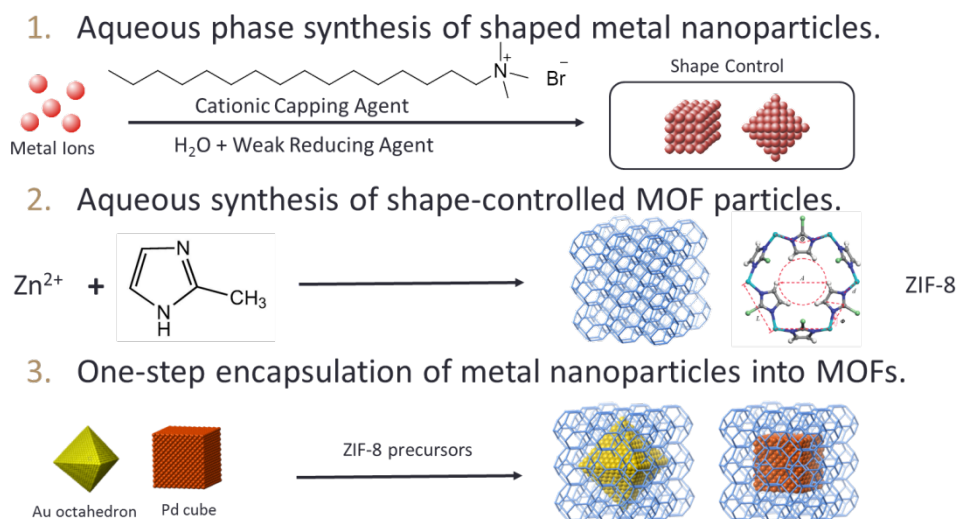


**Figure 3.** Overview of the synthesis of metal nanoparticles, cubic ZIF-8 particles, and Pd/Au@ZIF-8 core-shell nanoparticles.

## 2.1 Room Temperature Synthesis of Cubic ZIF-8 Nanoparticles in Aqueous Condition

The synthesis of cubic ZIF-8 nanoparticles was carried out following the previous report with some modifications.<sup>132</sup> 144  $\mu\text{L}$  0.01 M CTAB aqueous solution was added into 1 mL 1.32 M 2-methylimidazole aqueous solution and the mixture was stirred at 500 rpm for 5 minutes without any heating. Then 1 mL 24 mM  $\text{Zn}(\text{NO}_3)_2 \cdot 6\text{H}_2\text{O}$  aqueous solution was injected into the mixture and the whole solution was stirred for another 5 minutes at 500 rpm. The solution was then left undisturbed at room temperature for 3 hours. During the reaction, the solution turned from semi-transparent to opaque milky white. The reaction solution was divided into two portions in 1 mL

centrifuge tube. The formed ZIF-8 particles was spun down at 5,000 rpm for 10 minutes, washed once by methanol, and finally re-dispersed in methanol. For synthesis of ZIF-8 nanocubes with different sizes from around 150 nm to 60 nm, 96/120/144/168/192  $\mu\text{L}$  0.01 M CTAB was added accordingly.

## 2.2 Synthesis of Various Types of Noble Metal Nanoparticles

**30 nm Pd nanocubes:** The synthesis was carried out following the previous report with some modifications.<sup>24, 133</sup> 50 mg CTAB was dissolved in 9.3 mL d. i.  $\text{H}_2\text{O}$  in a 20 mL borosilicate glass vial, 0.50 mL 0.01 M  $\text{H}_2\text{PdCl}_4$  aqueous solution was then added into the CTAB solution. No potassium iodide solution is added. After heating for 5 minutes at 95 °C in mineral oil bath with gentle stirring at 200 rpm, 0.20 mL 0.04 M freshly prepared ascorbic acid aqueous solution as reducing agent was injected into the vial. The reaction solution will turned to brownish black immediately after the injection of ascorbic acid, indicating the reduction of Pd precursors. The solution was left at 95 °C for another 30 minutes and then cooled down to room temperature. The formed Pd particles were spun down at 8000 rpm for 15 minutes and re-dispersed in d. i.  $\text{H}_2\text{O}$ .

**50 nm Au octahedron:** The synthesis was carried out following the previous report with some modifications.<sup>134</sup> 550 mg CTAB was dissolved in 97 mL d. i.  $\text{H}_2\text{O}$  in beaker, following by adding 2.50 mL 0.01 M  $\text{HAuCl}_4$  and 0.50 mL 0.1 M trisodium citrate aqueous solutions. The mixture solution was transferred into a 200 mL pressure vessel,

then sealed the pressure vessel and heated it to 110 °C in oven. Keep at this temperature for 24 hours before cool it down to room temperature. The reaction solution turned from yellow-orange color (mixture of precursors) to purple-pink (Au octahedra product). The formed Au octahedra were spun down at 6000 rpm for 20 minutes and re-dispersed in d. i. H<sub>2</sub>O.

**50 nm Au nanocubes:** The synthesis was carried out following the previous report with some modifications.<sup>135</sup> For the synthesis of Au seeds, 0.25 mL 0.01 M HAuCl<sub>4</sub> was firstly added into 7.50 mL 0.10 M CTAB aqueous solution. 0.60 mL 0.01 M freshly prepared ice-cold NaBH<sub>4</sub> solution was then injected into the Au solution, followed by rapid inversion mixing for 2 minutes. The Au seed solution was aged for 1 hour at 30 °C to prevent the precipitation of CTAB. 0.20 mL 0.01 M HAuCl<sub>4</sub> was added into a 9.6 mL aqueous solution containing 0.0167 M CTAB. Then 0.95 mL 0.10 M fresh ascorbic acid was added, followed by addition of 5 μL 1:10 diluted Au seeds. The growth solution was gently mixed and left undisturbed for 1 hour. The formed Au particles were spun down at 6000 rpm for 20 minutes and re-dispersed in d. i. H<sub>2</sub>O.

### **2.3 Encapsulation of metal nanocrystals into ZIF-8 cube**

Similar to the synthesis of pure ZIF-8 nanocubes, 144 μL 0.01 M CTAB aqueous solution was added into 1 mL 1.32 M 2-methylimidazole aqueous solution and the mixture was stirred at 500 rpm for 5 minutes. Then 1 mL 24 mM Zn(NO<sub>3</sub>)<sub>2</sub>·6H<sub>2</sub>O aqueous solution was injected. Ten seconds after the addition of Zn(NO<sub>3</sub>)<sub>2</sub>·6H<sub>2</sub>O, 1

mL of the metal nanoparticle solution was injected into the mixture, while the metal nanoparticle solution concentrations had already been adjusted to 8 mmol/L (for Pd) and 4.8 mmol/L (for Au) metal content. The whole solution was stirred for another 5 minutes at 500 rpm. The reaction solution was then left undisturbed at room temperature for 3 hours, and the color turned from semi-transparent to opaque. The formed core-shell nanoparticles were spun down at 4000 rpm for 10 minutes, washed once by methanol, and finally re-dispersed in methanol. The procedures are illustrated in Figure 4. All the nanoparticles are washed by methanol two more times to remove the surfactant and dried in vacuum oven at 100 °C overnight before catalytic reactions.

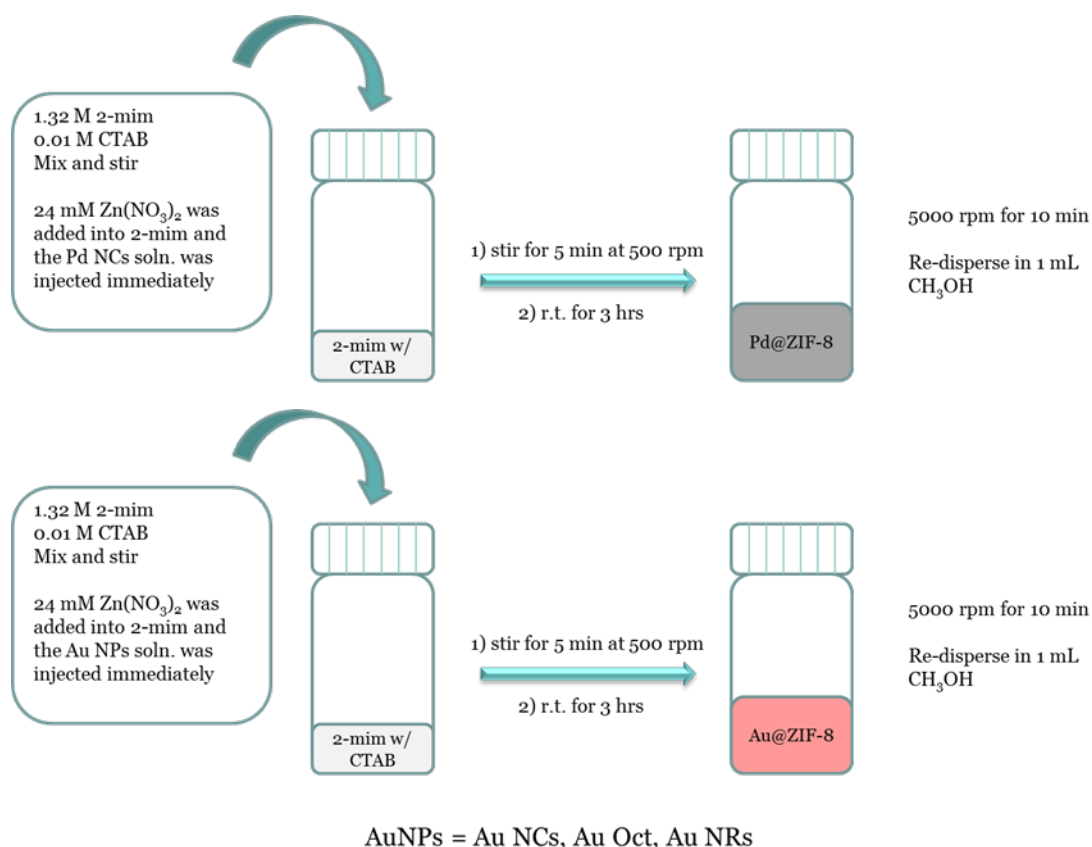


**Figure 4.** Scheme illustrates the encapsulation of Pd/Au nanoparticles into cubic ZIF-8.

## 2.4 Coating of mesostructured silica layer

**ZIF-8@mSiO<sub>2</sub>:** After the synthetic solution was spun down to get the formed ZIF-8, the nanocubes were re-dispersed in a mix solution which contained 1.8 mL NaOH aqueous solution and 0.2 mL ethanol, with the pH of the solution had already been adjusted to 11. Then 0.2 mL 0.01 M CTAB solution was added to the mix solution and the solution was put into a 50 °C water bath and pre-heated for 5 minutes. 10 µL TEOS was injected into the solution. The solution was left undisturbed for 1 hour in water bath. The formed core-shell nanoparticles were spun down at 5000 rpm for 10 minutes, washed by methanol, and re-dispersed in methanol. For the generation of hollow *mSiO<sub>2</sub>* cages, 1 M HCl solution was introduced to the core-shell particles to decompose the ZIF-8 and form the hollow cages.

**Pd@ZIF-8@mSiO<sub>2</sub>:** The synthesis of Pd@ZIF-8@mSiO<sub>2</sub> was similar to the synthesis of ZIF-8@mSiO<sub>2</sub>. Instead of using pure ZIF-8 nanocubes, Pd@ZIF-8 nanocubes were used for the mesoporous silica coating. 0.2 mL 1 M HCl was introduced to 1 mL particle solution to etch away the ZIF-8 layer and generate the Pd@mSiO<sub>2</sub> yolk-shell nanoparticles.

## 2.5 Overgrowth of MOF on pure MOF, and metal@MOF particles

The cubic ZIF-8 with size larger than 100 nm can be synthesized via a seed mediated

growth in aqueous solution. 144  $\mu\text{L}$  0.01 M CTAB aqueous solution was added into 1 mL 1.32 M 2-methylimidazole aqueous solution and the mixture was stirred at 500 rpm for 5 minutes. Then 1 mL 24 mM  $\text{Zn}(\text{NO}_3)_2 \cdot 6\text{H}_2\text{O}$  aqueous solution was injected, followed by the addition of 0.2 mL 100 nm ZIF-8 seed solution (concentration adjusted to 24.4 mmol/L) and stirring for another 5 minutes. The solution was then left undisturbed at room temperature for 1 hour, result in 250 nm cubic ZIF-8 nanoparticles. ZIF-8 cubes with size around 400 nm can be obtained by repeating these steps and use 250 nm ZIF-8 as seed.

Cubic ZIF-67 can also be synthesized in a similar method, just replace  $\text{Zn}(\text{NO}_3)_2 \cdot 6\text{H}_2\text{O}$  with  $\text{Co}(\text{NO}_3)_2 \cdot 6\text{H}_2\text{O}$ , while keeping all the other parameters unchanged. The reaction solution is cloudy and has the color of bright purple. Then ZIF-67@ZIF-8, ZIF-8@ZIF-67 core-shell structures consists of two kinds of MOFs, or ZIF-67@ZIF-8@ZIF-67, ZIF-8@ZIF-67@ZIF-8 sandwich structures can be also obtained in a similar way.

Solid or porous rhombic dodecahedral ZIF-8 particles can also be obtained via a seed mediated growth in methanol. 2.5 mL 30 mM 2-methylimidazole methanolic solution were mixed with 2.5 mL 30 mM  $\text{Zn}(\text{NO}_3)_2 \cdot 6\text{H}_2\text{O}$  methanolic solution in a glass vial. Then 0.2 mL 24.4 mmol/L methanolic solution contains 100 nm ZIF-8 seed was added. By varying the reaction time and water amount, we can synthesize solid or porous rhombic dodecahedral ZIF-8 particles.

### **Chapter 3: Characterization and Analysis**

### **3.1 Structures and Compositions of metal@MOF core-shell nanocrystals**

The transmission electron microscopy (TEM) and scanning electron microscopy (SEM) images show that the uniform Pd nanocubes, Au octahedra, and cubic ZIF-8 nanocrystals were synthesized (Figure 5). The Pd nanocubes and Au octahedra have the particle size of ~30 nm and ~50 nm, respectively. The particle size of cubic ZIF-8 can be tuned from ~60 nm to ~150 nm by varying the amount of the surfactant CTAB. The high concentration of surfactant can slow down the crystallization of ZIF-8 and thus constrain the increase of particle size. The cubic structure enclosed by six {100} facets has the simple geometric morphology that can benefit the exploration of the alignment. The metal nanoparticles we chose are Pd and Au because of their potential applications in catalysis and plasmonics.

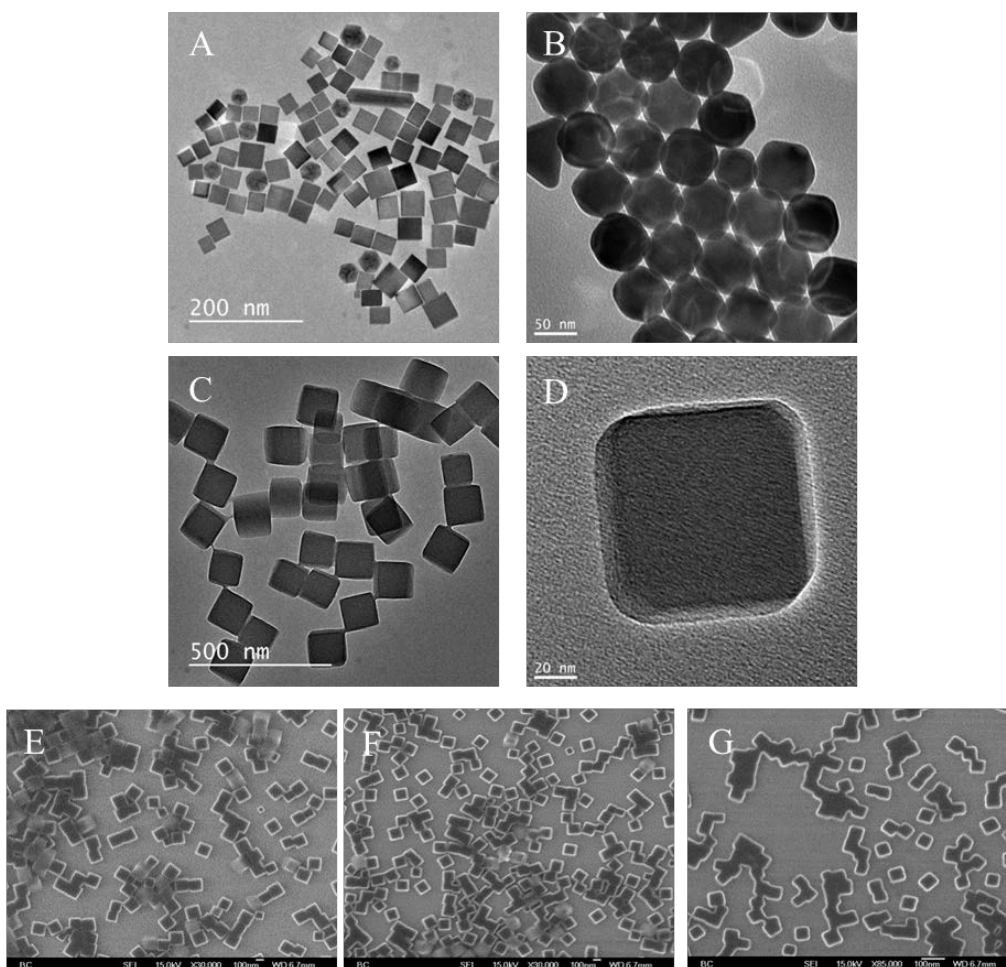


**Figure 5.** TEM images of Pd nanocube (A); Au octahedron (B); ZIF-8 nanocube (C, D). SEM images of ZIF-8 with particle size from 150 nm to 60 nm (E, F, G).

To synthesize metal@ZIF-8 core-shell nanocomposites, metal nanocrystals are synthesized first and then introduced to the ZIF-8 synthesis solution about 10 seconds after the ZIF-8 precursors are mixed (Figure 4). The SEM and TEM images of Pd@ZIF-8 show that metal cores are individually incorporated into the cubic single crystalline ZIF-8 shell (**Figure 6**). In most cases, every cubic ZIF-8 crystal contains only one metal nanocrystal that locates right in the center. The size distribution of

nanocomposites is very narrow with most particles fall in the range from 90 to 110 nm (Table 2). Few, if any, free-standing Pd nanocrystals were found outside the ZIF-8 cubes without MOF coating. These metal particles tend to aggregate and precipitate out of the solution. A small number of empty ZIF-8 cubes were also observed but could be easily removed by differential centrifugation. The morphology of the metal cubes in the core was fully preserved, with no signs of sintering or etching.

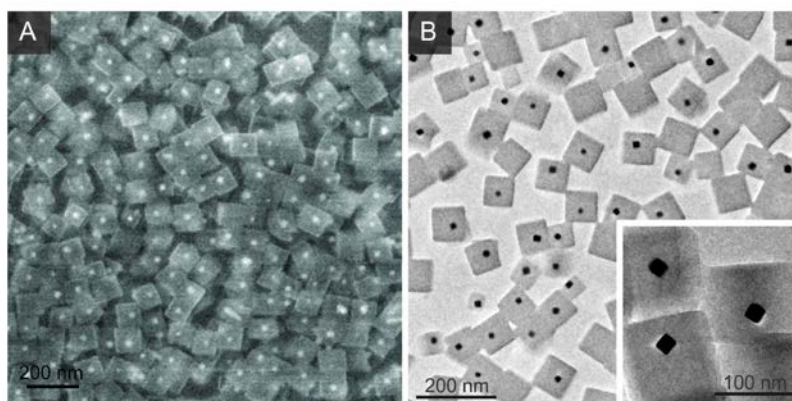


**Figure 6.** (A) SEM and (B) TEM images of Pd@ZIF-8 core-shell nanostructures.

As mentioned before, particle size of MOF can be modified by varying the CTAB amount, thus in this type of core-shell structure, the ZIF-8 shell thicknesses are tuned from ~35 to 60 nm (Figure 7). This shell thickness control could be further applied for the study of diffusion behaviors of different molecules.

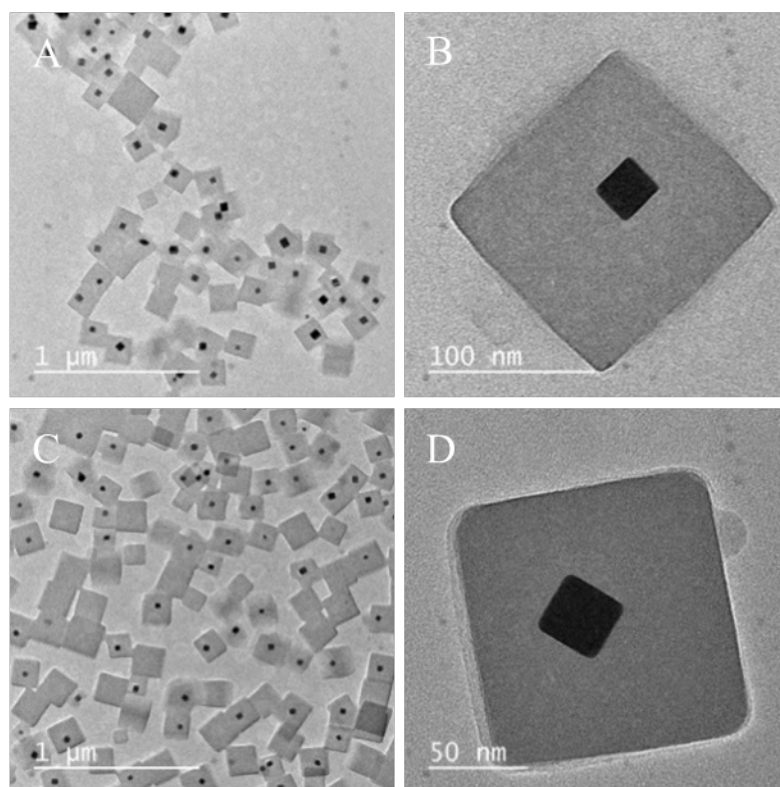


**Figure 7.** TEM images of Pd@ZIF-8 with different average shell thicknesses: 60 nm (A, B); 35 nm (C, D). With high concentration of CTAB, the growth of ZIF-8 was affected and sometimes incomplete encapsulation can be observed.

The crystal structures and chemical compositions of the core-shell nanocomposites were confirmed by powder X-ray diffraction (PXRD) (Figure 8) and inductively coupled plasma optical emission spectroscopy (Table 1). XRD pattern shows the signature peaks of both metal and ZIF-8, confirming the presence of these substances. The significant differences in intensity or broaden peak that shown in some previous studies are not observed here, indicating the good crystallinity of the metal and MOF. The loading amount of metal in previous reports is generally below 10%, while our results show a loading amount reaches as high as 25%, and it can be tuned easily by

different MOF shell thickness.

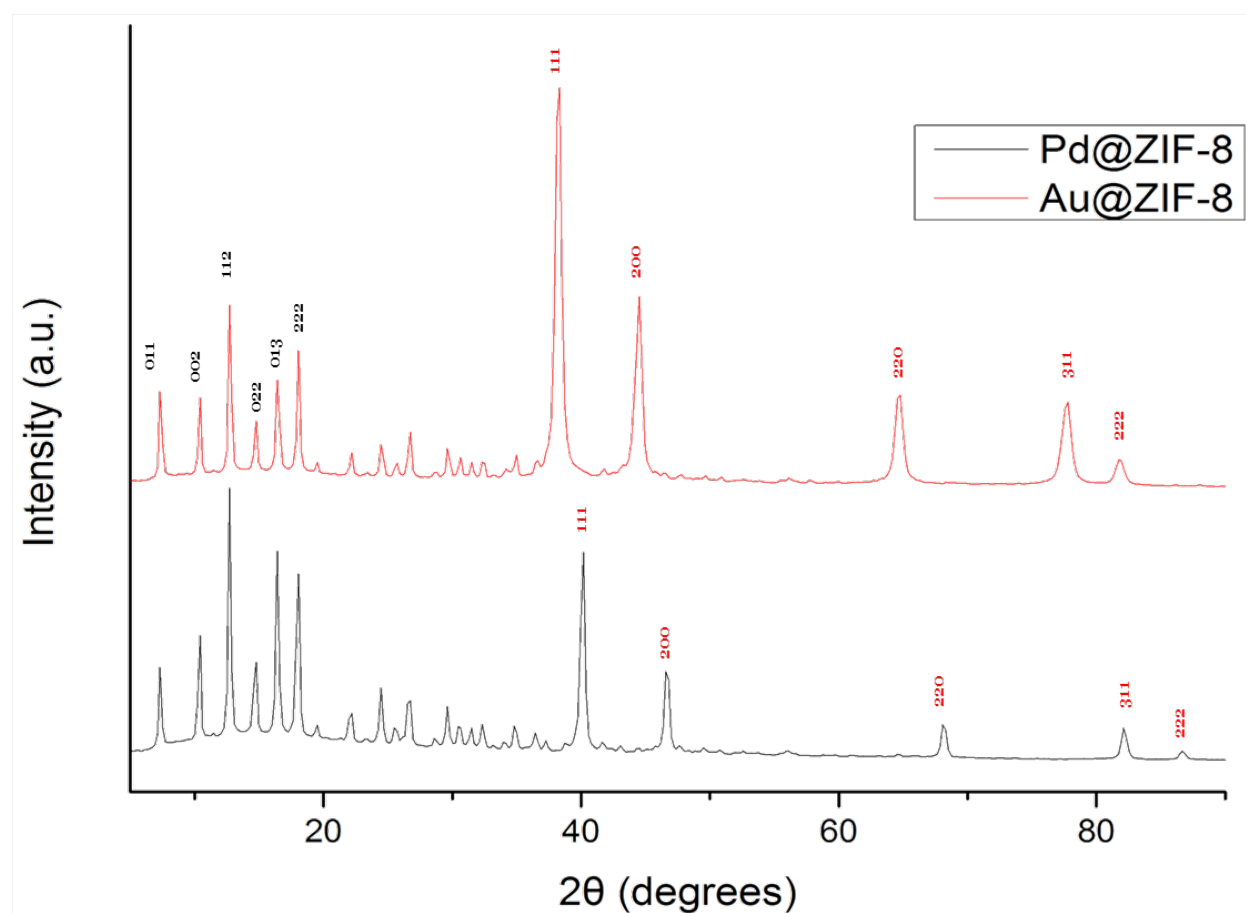


**Figure 8.** Powder XRD pattern of Au@ZIF-8 and Pd@ZIF-8. Signature peaks of ZIF-8 shell (shown in black 011, 002, 112, 022, 013, 222 in the range of  $2\theta= 5 - 35^\circ$ ) and Pd/Au core (shown in red 111, 200, 220, 311 in the range of  $2\theta= 35 - 90^\circ$ ) were both observed in the same PXRD pattern, which indicated the co-existence of the MOF and metal.

Sample	Pd@ZIF-8	Au@ZIF-8	Pure ZIF-8
Molal concentration:	Pd: 0.413	Au: 0.365	Zn:0.511
mg/mL	Zn: 0.643	Zn: 0.410	

Molar concentration: mmol/L	Pd: $3.88 \times 10^{-3}$ Zn: $9.83 \times 10^{-3}$	Au: $1.85 \times 10^{-3}$ Zn: $6.27 \times 10^{-3}$	Zn: $7.82 \times 10^{-3}$
metal/Zn molar ratio	39.5%	29.5%	N/A
Yield	Pd 70.8%	Au 88.9%	N/A
Loading amount (metal/ZIF-8)	18.3 wt%	25.3 wt%	0

**Table 1.** Elemental analysis by ICP-OES. The loading amount of metal in ZIF-8 was relatively high. No significant loss of metal nanoparticles during the ZIF-8 coating was observed.

To demonstrate this colloidal synthesis is a general way of bridging two materials with different lattice scales, CTAB was further utilized to direct the overgrowth of the MCM-41 type mesostructured silica ( $m\text{SiO}_2$ ) on the external surface of ZIF-8 cube (Figure 9). We believe the self-assembled layer of CTAB molecules served as a structure directing agent (SDA) of the mesostructure, and it bridged the mesoporous silica and nanoporous ZIF-8 as well. The ZIF-8 can be etched by hydrochloric acid, leaving a free-standing cubic hollow mesostructured silica shell. This strategy utilized MOF crystals as hard templates to synthesize quality hollow mesoporous silica nanocage in large scale.

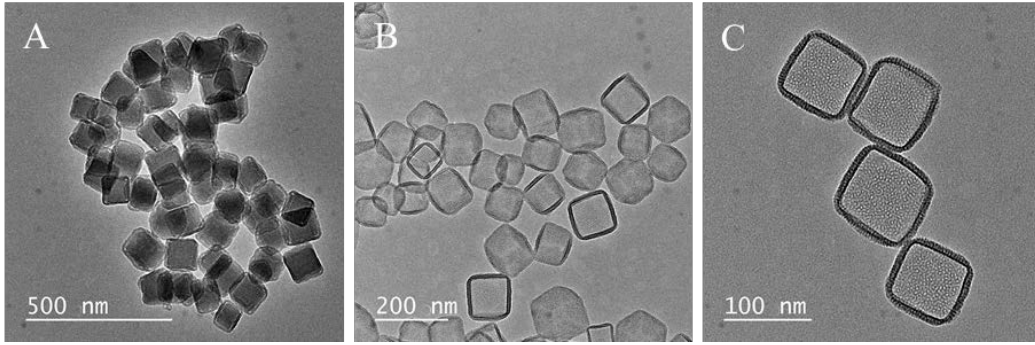


**Figure 9.** TEM images of mesoporous SiO<sub>2</sub> synthesis without Pd nanocubes, before acid treatment (A), and after acid treatment (B, C).

By adding tetraethyl orthosilicate (TEOS) into the colloidal Pd@ZIF-8 nanocomposite solution with the presence of CTAB, a uniform layer of silica mesostructure overgrew on the ZIF-8 (Figure 10). A magnified TEM image shows that all the mesopores of silica are perpendicular to the {100} surface of ZIF-8 cubes. After the acid treatment, ZIF-8 was etched away and Pd@mSiO<sub>2</sub> yolk-shell nanostructures were obtained. This could also be a novel strategy to fabricate yolk-shell particles by utilizing MOF as sacrificial templates.

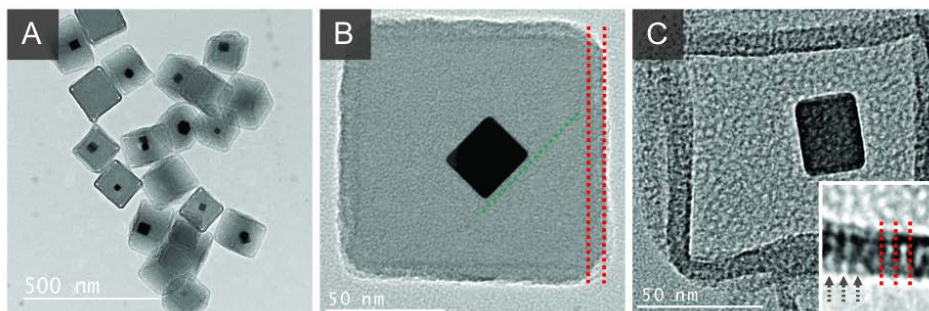


**Figure 10.** TEM images of (A, B) Pd@ZIF-8@mSiO<sub>2</sub> with alignment from atomic to

mesoscopic scales and (C) Pd@mSiO<sub>2</sub> yolk-shell nanocomposite with cylindrical mesostructured channels.

Small-angle X-ray scattering (SAXS) patterns confirm the crystal structure of the metal, nanoporous structure of ZIF-8, and mesostructure of silica (Figure 11). Three different materials with crystal lattice from atomic scale (Pd nanocrystal), microscale (ZIF-8 with micropores), to mesoscale (*m*SiO<sub>2</sub>) are combined within one single particle.

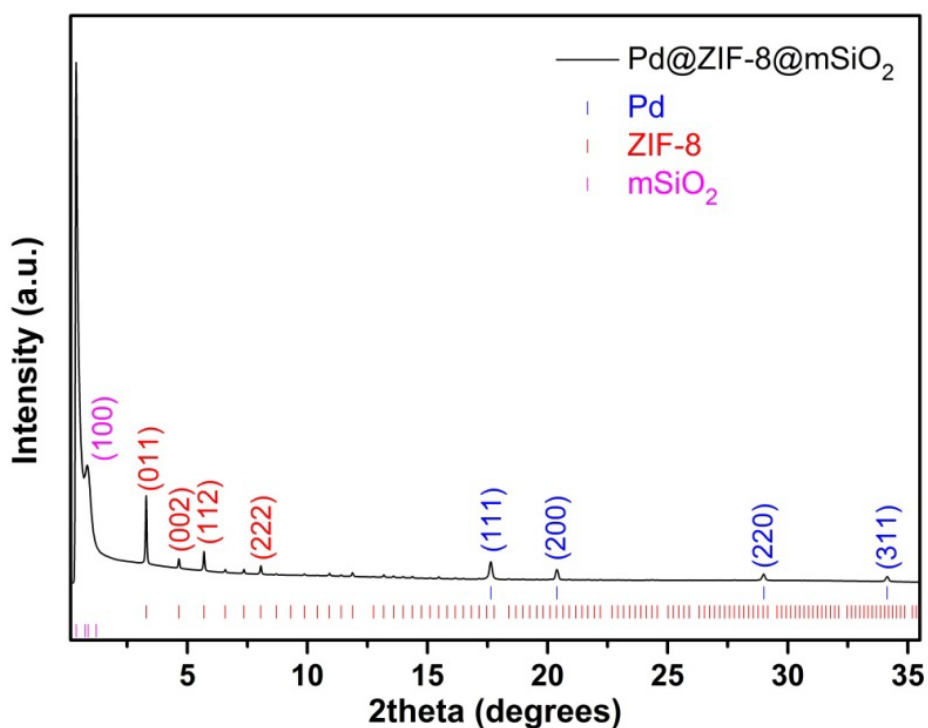


**Figure 11.** SAXS/PXRD of Pd@ZIF-8@mSiO<sub>2</sub> (x-ray wavelength 0.68881 Å, capillary diameter 0.3 mm, exposure time 150 s). Signature peaks of *m*SiO<sub>2</sub>, ZIF-8 and Pd could be observed in the same graph, which indicated the existence of all three components.

In the absence of CTAB molecules, the formation of either solid or mesostructured silica layer was not observed (Figure 12). After the removal of ZIF-8 by acid treatment, the cylindrical-oriented mesostructures can be easily observed, which indicates the CTAB layer even provides a certain degree of alignment during the cooperative self-assembly of the mesostructure. (Figure 10)

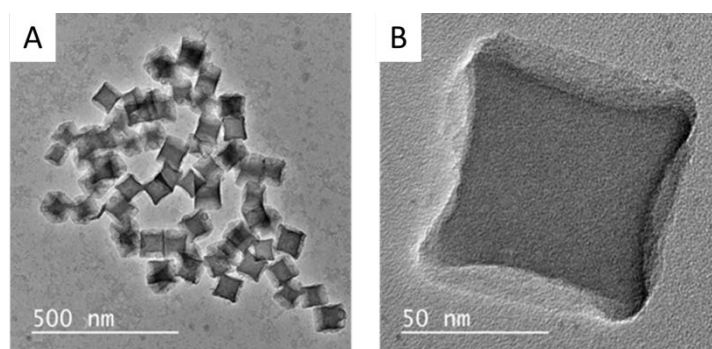


**Figure 12.** TEM images of  $m\text{SiO}_2$  synthesis without CTAB. No coating on ZIF-8 was observed, and only formed small silica nanoparticles could be seen on the background.

### 3.2 Alignments between metal core and MOF

The alignments between metal nanocrystals and ZIF-8 are examined by the magnified TEM images and illustrated by 3D crystal modelling (Figure 13). Since both the metal and ZIF-8 cubes are enclosed by six  $\{100\}$  surfaces, it is easier to reveal the lattice alignment based on the relative orientations between them. Most of the nanocomposites show the same alignment. In figures 13, two view directions of this alignment are shown, two sets of  $\{100\}$  planes of the metal align with two sets of  $\{110\}$

planes of ZIF-8, respectively. The 3D modeling of the projections in the [100] and [010] view directions of ZIF-8 are in good accordance with the TEM images.

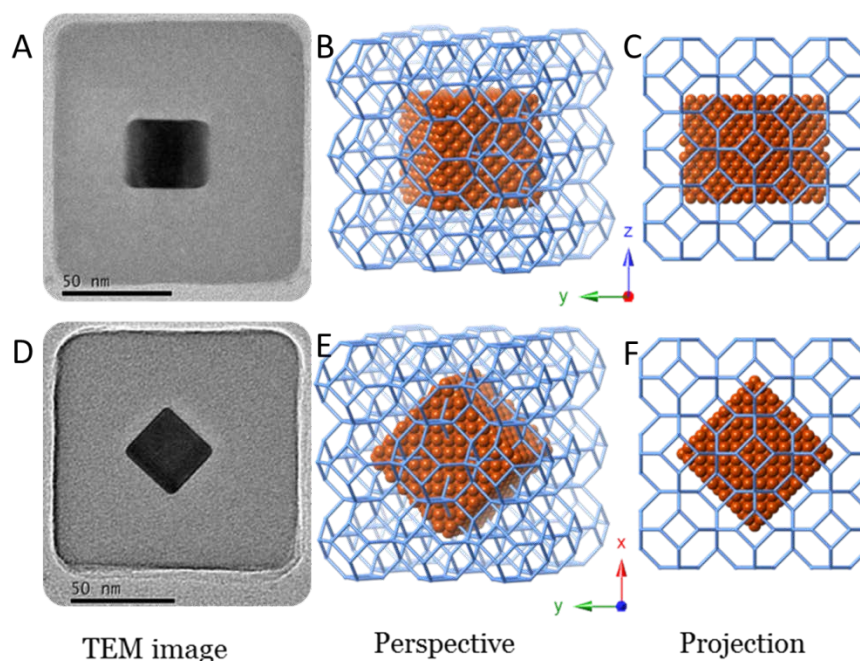


**Figure 13.** TEM images of Pd@ZIF-8 (A, D). Perspective view of the 3D models (B, E). Projections of the 3D modelling that match the TEM image well (C, F).

To further investigate the alignment, we tried to extend the range of this method. Au octahedra with size around 50 nm are used as metal core, and other conditions remain unchanged. To our surprise, the {100} planes of metal still align with the {110} planes of ZIF-8 shell, although the Au octahedra are mainly enclosed by eight {111} surfaces. Two view directions are shown in Figure 14. In the ZIF-8 [100] and [010] view directions, the respective rhombic and square-shaped cross sections with radial patterns along the diagonal were observed.

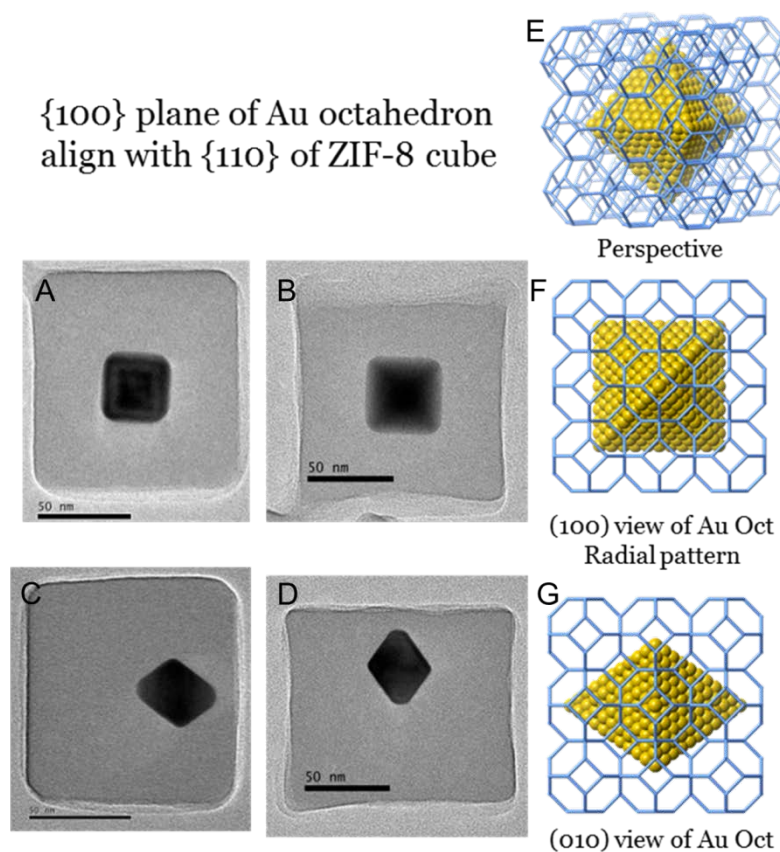


**Figure 14.** TEM images and corresponding 3D modelling of Au@ZIF-8 core-shell nanoparticles. [100] view of TEM images and projection (A, B, F), [010] view of TEM images and projection (C, D, G). Perspective view (E).

A small portion of the nanocomposites have the alignment between  $\{100\}$  planes of the metal and  $\{100\}$  planes of ZIF-8 (Figure 15). A possible explanation is the energy difference between these two kinds of alignment is not very large. Thus metal $\{100\}$ -MOF $\{100\}$  alignments can also be observed despite the dominant metal $\{100\}$ -MOF $\{110\}$  alignment.

(100) of Pd NC aligned with (100) of ZIF-8

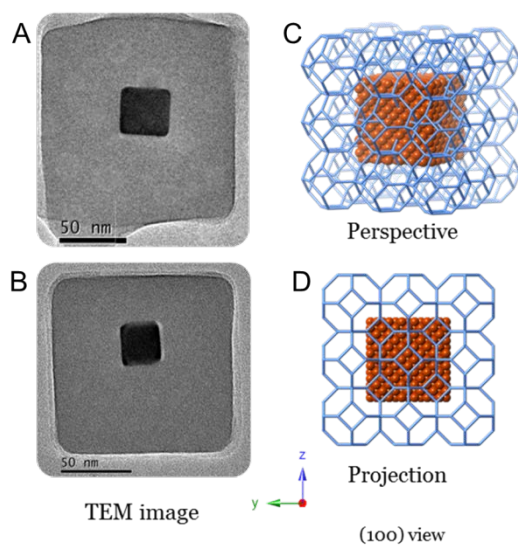
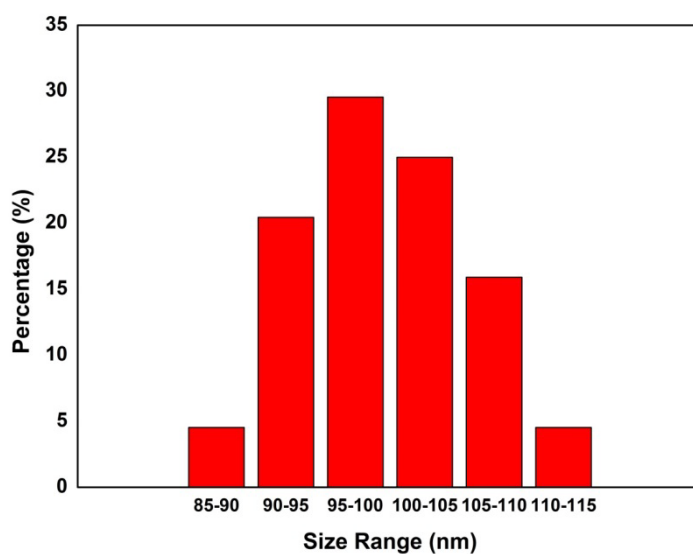


**Figure 15.** TEM image (A, B) and 3D modeling of Pd {100} aligned with ZIF-8 {100} (perspective: C, projection: D).

The percentage of core-shell nanoparticles with these two alignments can be found in Table 2. No other alignment orientations are observed in our products.



<b>Alignment</b>	<b>ZIF-8 {110} align with Pd {100}</b>	<b>ZIF-8 {100} align with Pd {100}</b>
<b>Particle numbers</b>	34	10
<b>Percentage</b>	77.3%	22.7%

**Table 2.** Particle size distribution and mis-oriented particle percentage.

### 3.3 Catalytic Applications in alkene hydrogenation

Size selective hydrogenation reactions of different alkenes were carried out to further confirm that the metal nanocrystals were encased in ZIF-8, as well as to demonstrate their potentials as selective catalyst. Figure 16 illustrates how the core-shell catalyst has size selectivity towards different reactant molecules. The pore size of ZIF-8 is 11.6 Å while the aperture size is only 3.4 Å. Only reactant molecules with size smaller than the aperture size of ZIF-8 can pass through the porous shell and reach the metal surface thus undergo hydrogenation.

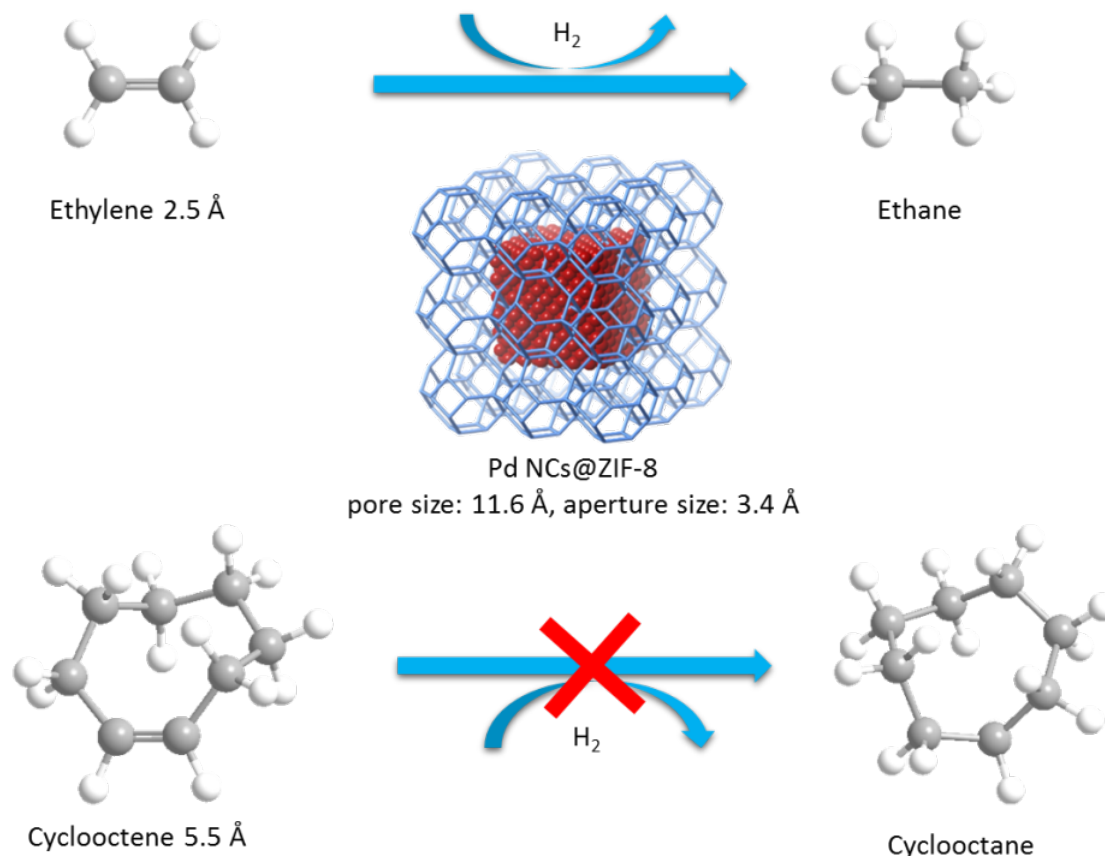


**Figure 16.** Illustration of size selective alkene hydrogenation reaction catalyzed by Pd@ZIF-8 core-shell nanoparticles.

The Pd@ZIF-8 nanocomposites were compared with a control sample containing the same amount of Pd. Instead of being embedded inside the MOF, the Pd nanoparticles in the control experiment are deposited on the external surface of ZIF-8 crystals. After intensive washing by methanol to remove the surfactant CTAB, the morphology of the core-shell catalyst particles remains unchanged. From Table 3 we can conclude that both samples show activities in ethylene hydrogenation, because the small molecular size of ethylene allows it penetrate ZIF-8 shell without any obstacles. No activity was

observed for *cis*-cyclooctene hydrogenation over the Pd@ZIF-8 sample, while appreciable activity was observed over the control sample. This is because the size of cyclooctene molecules is much larger than the aperture size of ZIF-8, only the Pd particles in control experiment can catalyze the hydrogenation. These selective hydrogenation results proved that the all the metal nanocrystals are encased inside ZIF-8 cube, and no fractures or cracks exist in the single crystalline ZIF-8 shell. Otherwise, Pd@ZIF-8 will not be able to show the size selectivity.

	Pd@ZIF-8	Pd on ZIF-8
Ethylene Hydrogenation		
Activity ( $\text{mol} \cdot \text{g}_{\text{pd}}^{-1} \cdot \text{s}^{-1}$ )	$3.06 \times 10^{-2}$	$3.34 \times 10^{-2}$
Ea (kJ/mol)	41.1	40.8
Cyclooctene Hydrogenation		
Activity ( $\text{mol} \cdot \text{g}_{\text{pd}}^{-1} \cdot \text{s}^{-1}$ )	Not detectable	$2.96 \times 10^{-6}$
Ea (kJ/mol)	N/A	37.4

**Table 3.** Heterogeneous catalysis for Pd@ZIF-8 and Pd on ZIF-8 support: hydrogenation of ethylene and cyclooctene, activity and activation energy.

The catalytic reactions are carried out as following procedures.<sup>113, 136</sup> 1.95 mg Pd@ZIF-8 (0.7 wt% Pd) and 2.09 mg Pd on ZIF-8 (0.72 wt% Pd) samples were

diluted with low surface area quartz and loaded into glass reactors. Temperature was controlled by a furnace (Carbolite) and PID controller (Digi-Sense) with a type-K thermocouple. Gas flows, including helium, hydrogen gas and ethylene were regulated using calibrated mass flow controllers. The desired partial pressure of *cis*-cyclooctene was achieved by bubbling helium through the liquid and assuming saturation. For all reactions, gas composition was analyzed with a mass spectroscope (MKS special V2000P). The turnover frequency of *cis*-cyclooctene hydrogenation is normalized by using ethylene hydrogenation. All the reaction rate and activation energy measurements were conducted at differential conditions (all conversions,  $X < 10\%$ ). The activation energies were measured at 293-333 K.

## **Chapter 4: Discussion**

### **4.1 Growth Mechanism of Metal@ZIF-8**

To the best of our knowledge, this type of metal@ZIF-8 nanocomposite is the first example that exhibits specific lattice alignments between the metal core and porous material shell. We have proposed a growth mechanism that illustrated in Figure 2 as we discussed the motivation of this research. The first step is the formation of small ZIF-8 crystal nuclei enclosed by low surface energy  $\{110\}$  facets in the solution, which is described as “fast nucleation” in nanoscience. Then one single ZIF-8 crystal nucleus selectively attaches to the  $\{100\}$  facet of metal via the bridging CTAB layer

and generates a ZIF-8 {110} to metal {100} interface, due to the fact {110} and {100} facets are the most stable of ZIF-8 and Pd/Au, respectively. Then the ZIF-8 shell continues to grow exclusively on this orientated crystal nucleus to capture the metal nanocrystal, instead of through a layer-by-layer conformal overgrowth mechanism. This one metal core to one MOF nucleus attachment leads the one-in-one single-crystalline structure. The key step of this mechanism, ZIF-8 nucleus selectively attached on the metal {100} facet, is reasonable in the metal cube case because of the dominant {100} facets of the metal cubes. The octahedral geometry allows for a few, small {100}-terminated surfaces, these of which are exclusively located at the vertices, and arise from truncation due to the increase in under-coordinated (higher surface energy) atoms at the apex. The {100} metal facets still serve as the anchoring site for the tiny ZIF-8 crystal nucleus, despite they are not dominant in the octahedral morphology. The previous results from extensive studies in self-assembled monolayer (SAM) system could help to explain this highly selective attachment. Huo and co-workers<sup>137</sup> had shown that the ZIF-8 nucleus on the SAM is very sensitive to the metal surface because the orientation of nuclei is determined by the distance between the self-assembled molecules, and the distance of the molecules is determined by the surface metal lattices. In this study, self-assembled molecular layer of CTAB on the {100} surface of metal nanocube exhibits structurally advantages for the ZIF-8 nucleus anchoring compared with other facets.

A direct evidence to prove our proposal is the TEM images of metal@ZIF-8 at

different reaction stages (Figure 17). In the early stage of the reaction (less than 2 minutes), a small ZIF-8 nanocrystal is attached to the vertex of Au octahedron/Pd nanocube, and specific alignments had already existed in the one-to-one combination. As the growth continued, the alignments were fully preserved and eventually resulted in the formation of metal@MOF core-shell nanocomposites with the interface alignments.

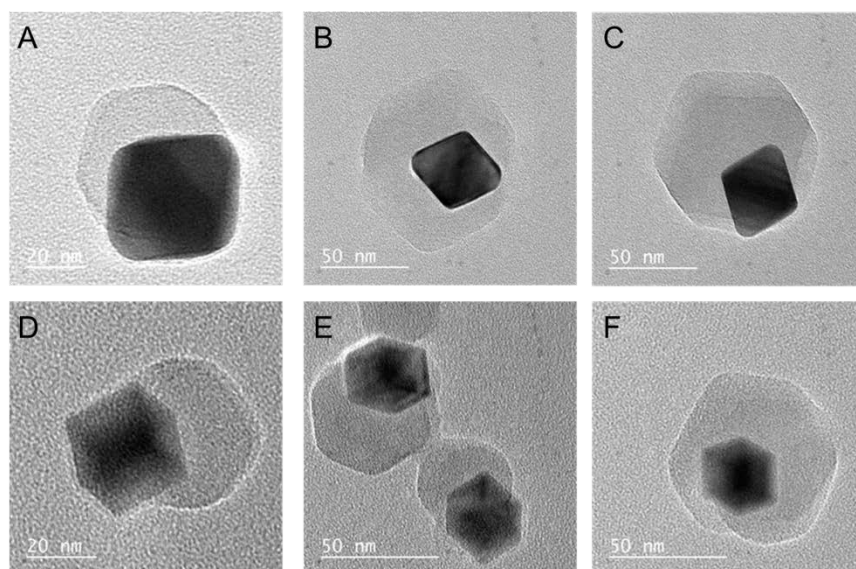


**Figure 17.** TEM images of Au@ZIF-8 (A, B, C) and Pd@ZIF-8 (D, E, F) that were arrested at early stage of the reaction.

## 4.2 Role of Surfactant in the Overgrowth of ZIF-8 on Metal

Due to the important role surfactant played in the overgrowth, a detailed study is necessary for fundamental understanding. Surface-enhanced Raman scattering (SERS)

was carried out during the synthesis of Au octahedra@ZIF-8 core-shell nanoparticles, to confirm the existence of CTAB layer through different reaction stages. Similar intensities of the main SERS signal, -CH<sub>2</sub>- twisting mode of CTAB at 1266 cm<sup>-1</sup> (Figure 18) have been observed before the ZIF-8 coating, during the overgrowth, and after the complete encapsulation. As the SERS intensity is highly dependent on the amount of probe molecules present on the surface of Au, we may conclude that the amount of CTAB near the surfaces of the Au octahedra merely changed throughout the reaction. So CTAB molecules played an important role in the overgrowth of ZIF-8 on metal.

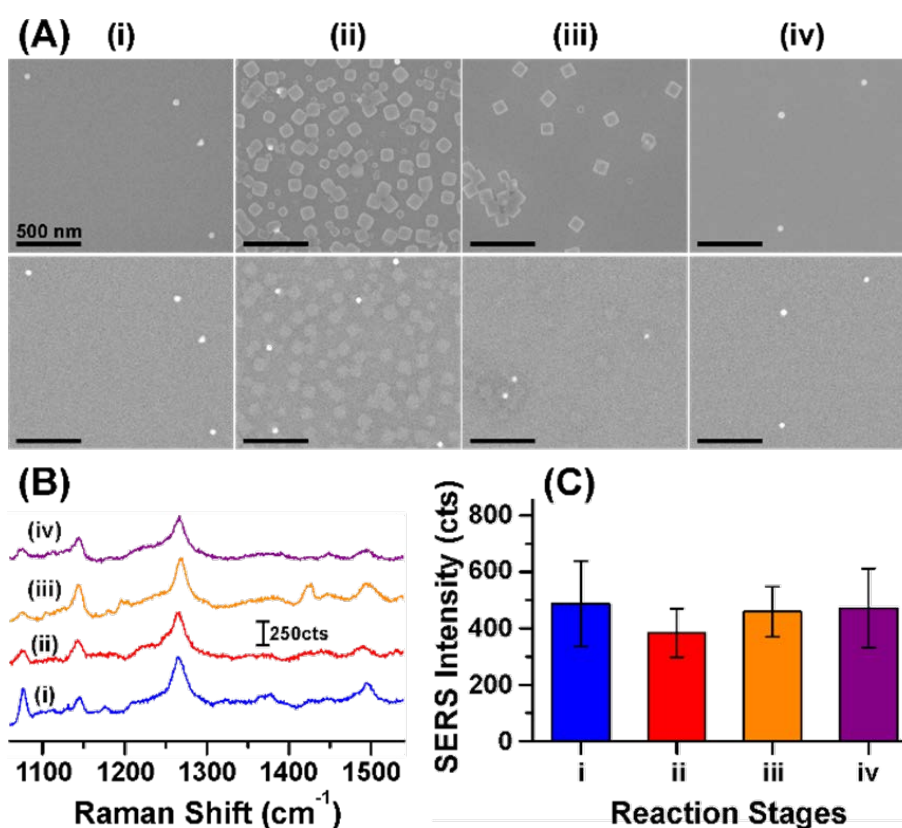


**Figure 18.** SEM images (A), Raman shift (B), and SERS intensity of four reaction stages.

Stage I: pure Au octahedron; Stage II: Au Oct partially encapsulated into ZIF-8; Stage III: Au Oct fully encapsulated into ZIF-8; Stage IV: Au Oct release to solution after acid digestion

Besides, metal nanocrystals capped by PVP instead of CTAB in methanolic solution were used for comparison. PVP is widely used to facilitate the encapsulation, but with less control. Multiple nanocrystals were encapsulated in one large ZIF-8 crystal and no specific alignment was observed. In addition, when the metal nanocrystals and precursors of ZIF-8 were mixed simultaneously, we may still observe the successful encapsulation but obtain only polycrystalline ZIF-8 shells rather than single crystal. (Figure 19) We proposed an explanation that when the metal nanocrystals are introduced into the synthesis solution before the formation of tiny nuclei of ZIF-8, the amorphous nuclei will randomly anchor on multiple spots of metal surface and continue to grow toward different directions. Eventually the anisotropic growth leads to the formation of polycrystalline ZIF-8 shells.

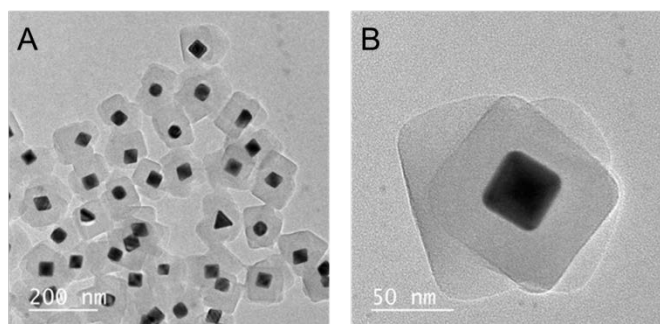


**Figure 19.** TEM images of Au octahedron@ZIF-8 with polycrystalline shell (A: Low

magnification, B: a single Au@ZIF-8 particle).

### 4.3 General strategy to synthesize multiple-layer core-shell/yolk-shell MOF nanostructures

After the success in colloidal synthesis of ZIF-8, we try to explore the generality of this strategy and apply it to other types of MOFs. ZIF-67, with cobalt ions as SBUs and 2-methylimidazole as organic linkers, shares the same structural characteristics with ZIF-8. We successfully synthesize cubic ZIF-67 with particle size around 100 nm in the similar colloidal conditions, simply replace zinc nitrate solution with cobalt nitrate. From the SEM images (Figure 20), we may conclude the size distribution is uniform and no signs of truncation or defects are observed regarding the morphology of ZIF-67 cubes.

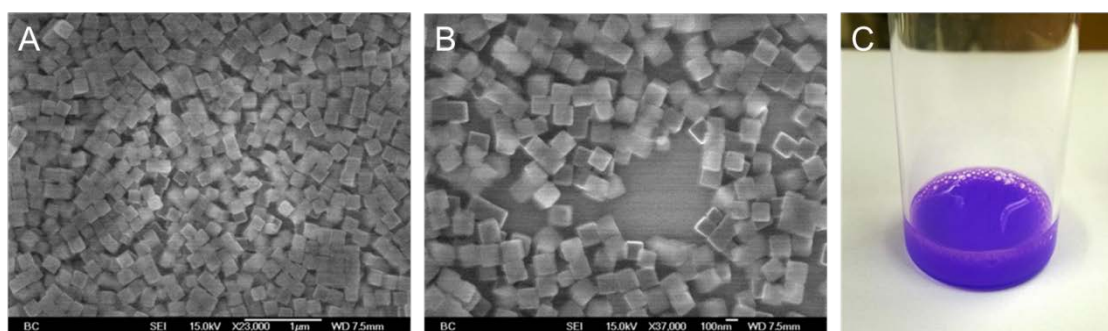


**Figure 20.** SEM images of ZIF-67 (A, B). Picture of the reaction solution shows the bright purple color of this Cobalt containing MOF (C).

Based on our previous experiments on ZIF-8, a seed-mediated growth can be applied to produce cubic MOF particles with size larger than 100 nm. For example, if we add the 100 nm ZIF-8 cubes as seeding solution into the synthesis solution of MOF, another layer of ZIF-8 can be directly overgrown around the seed to form 250 nm ZIF-8@ZIF-8 nanocubes, triple-layered ZIF-8@ZIF-8@ZIF-8 nanostructures can also be obtained by the same strategy, using 250 nm ZIF-8 cubes as seeds (Figure 21). Since ZIF-67 shares the same crystal structure with ZIF-8, a facile overgrowth is expected. Figure 21 shows the TEM images of ZIF-8@ZIF-67 and ZIF-67@ZIF-8, respectively. Further calcination will generate ZnO@Co<sub>3</sub>O<sub>4</sub> and Co<sub>3</sub>O<sub>4</sub>@ZnO core-shell structures, which attracts high interests in the studies of metal oxide semiconductors.

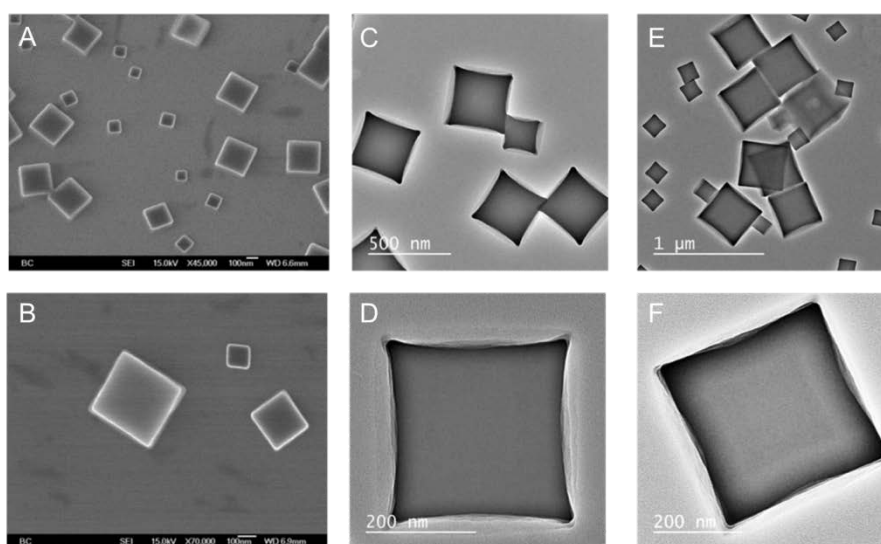


**Figure 21.** SEM images of ZIF-8@ZIF-8, ZIF-8@ZIF-8@ZIF-8 (A, B). TEM images of ZIF-8@ZIF-67 (C, D) and ZIF-67@ZIF-8 (E, F).

Another overgrowth method was carried out in methanolic solution containing the ZIF-8 precursors. The nucleation and formation of ZIF-8 in methanol is much slower than in water and rhombic dodecahedral (RD) morphology is generated instead of cubic shape, resulting in metal@ZIF-8 core-shell structures. Also, mesoscale porosity can also be observed in the RD particles resulting in a hollow or yolk-shell structure of pure ZIF-8 or metal@ZIF-8. (Figure 22) Careful calcination will generate the metal@porous carbon nanomaterials, which could be used in electrochemical catalysis.

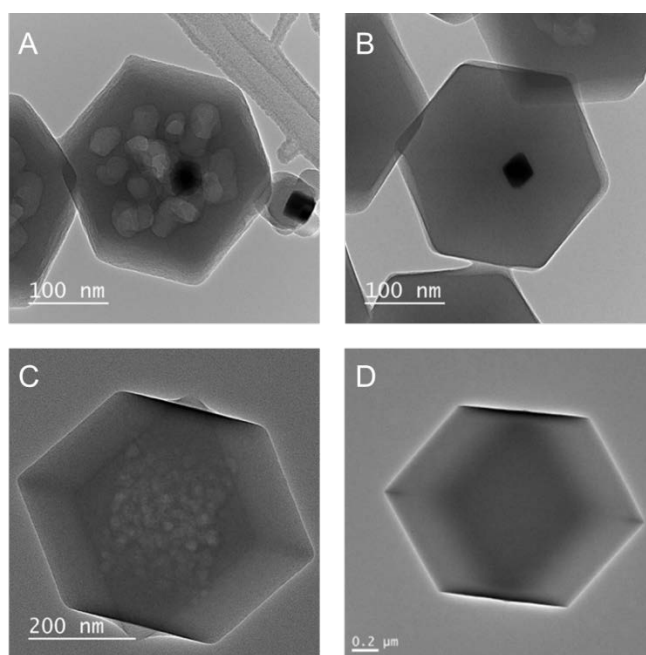


**Figure 22.** TEM images of Pd @ZIF-8@ZIF-8 (A), Au@ZIF-8@ZIF-8 (B), ZIF-8@ZIF-8 yolk-shell/core-shell nanoparticles (C, D).

## Chapter 5: Conclusion

In the recent years, significant progress has been made in the integration of metal nanocatalysts and nanoporous materials. From the stiff and solid zeolites to more flexible and modifiable MOFs, more and more advanced materials have been developed to combine with metal catalysts. The core-shell nanostructures consist of metal nanocrystals and crystalline MOFs exhibit great potential in heterogeneous catalysis and other applications. Following the “ship-around-bottle” or *de novo* approach, we have developed a new strategy to individually encase single metal nanocrystals into single-crystalline cubic ZIF-8 nanocubes with a specific lattice alignment. A third layer of mesostructured silica was also deposited on the metal@ZIF-8 nanocomposite surface with alignment by the same strategy. The self-assembled surfactant CTAB promotes the interaction between different materials, facilitates the overgrowth, and guides the lattice alignments. To the best of our knowledge, this is the first example of the use of self-assembled molecules in colloidal synthesis to align crystalline materials with lattice range from atomic scale to mesoscale. The alignment is essential for follow-up studies on the diffusion and orientation of molecules in such structures which will be investigated via spectroscopic analysis and catalytic experiments. Predictably, this type of core-shell structured functional material will be one of the promising heterogeneous catalysts in the future. Further sustained researches in mechanisms and applications are necessary for the study in material science and catalysis.



## Reference

1. George, S. M., Introduction: Heterogeneous Catalysis. *Chemical Reviews* **1995**, *95* (3), 475-476.
2. Zhang, S.; Nguyen, L.; Zhu, Y.; Zhan, S.; Tsung, C.-K.; Tao, F., In-Situ Studies of Nanocatalysis. *Accounts of Chemical Research* **2013**, *46* (8), 1731-1739.
3. Narayanan, R.; El-Sayed, M. A., Catalysis with transition metal nanoparticles in colloidal solution: Nanoparticle shape dependence and stability. *Journal of Physical Chemistry B* **2005**, *109* (26), 12663-12676.
4. Bell, A. T., The Impact of Nanoscience on Heterogeneous Catalysis. *Science* **2003**, *299* (5613), 1688-1691.
5. Grunes, J.; Zhu, J.; Somorjai, G. A., Catalysis and nanoscience. *Chemical Communications* **2003**, (18), 2257-2260.
6. Schlögl, R.; Abd Hamid, S. B., Nanocatalysis: Mature Science Revisited or Something Really New? *Angewandte Chemie International Edition* **2004**, *43* (13), 1628-1637.
7. Astruc, D.; Lu, F.; Aranzaes, J. R., Nanoparticles as Recyclable Catalysts: The Frontier between Homogeneous and Heterogeneous Catalysis. *Angewandte Chemie International Edition* **2005**, *44* (48), 7852-7872.
8. Lee, H.; Habas, S. E.; Kweskin, S.; Butcher, D.; Somorjai, G. A.; Yang, P., Morphological Control of Catalytically Active Platinum Nanocrystals. *Angewandte Chemie International Edition* **2006**, *45* (46), 7824-7828.
9. Bratlie, K. M.; Lee, H.; Komvopoulos, K.; Yang, P.; Somorjai, G. A., Platinum Nanoparticle Shape

- Effects on Benzene Hydrogenation Selectivity. *Nano Letters* **2007**, *7* (10), 3097-3101.
10. Habas, S. E.; Lee, H.; Radmilovic, V.; Somorjai, G. A.; Yang, P., Shaping binary metal nanocrystals through epitaxial seeded growth. *Nature Materials* **2007**, *6* (9), 692-697.
11. Park, J.; Joo, J.; Kwon, S. G.; Jang, Y.; Hyeon, T., Synthesis of Monodisperse Spherical Nanocrystals. *Angewandte Chemie International Edition* **2007**, *46* (25), 4630-4660.
12. Xiong, Y.; Wiley, B. J.; Xia, Y., Nanocrystals with Unconventional Shapes—A Class of Promising Catalysts. *Angewandte Chemie International Edition* **2007**, *46* (38), 7157-7159.
13. Lee, I.; Morales, R.; Albiter, M. A.; Zaera, F., Synthesis of heterogeneous catalysts with well shaped platinum particles to control reaction selectivity. *Proceedings of the National Academy of Sciences* **2008**, *105* (40), 15241-15246.
14. Tao, A. R.; Habas, S.; Yang, P., Shape Control of Colloidal Metal Nanocrystals. *Small* **2008**, *4* (3), 310-325.
15. Chen, J.; Lim, B.; Lee, E. P.; Xia, Y., Shape-controlled synthesis of platinum nanocrystals for catalytic and electrocatalytic applications. *Nano Today* **2009**, *4* (1), 81-95.
16. Lee, I.; Delbecq, F.; Morales, R.; Albiter, M. A.; Zaera, F., Tuning selectivity in catalysis by controlling particle shape. *Nat Mater* **2009**, *8* (2), 132-138.
17. Cao, A.; Lu, R.; Veser, G., Stabilizing metal nanoparticles for heterogeneous catalysis. *Physical Chemistry Chemical Physics* **2010**, *12* (41), 13499-13510.
18. Goesmann, H.; Feldmann, C., Nanoparticulate Functional Materials. *Angewandte Chemie International Edition* **2010**, *49* (8), 1362-1395.
19. Jia, C.-J.; Schuth, F., Colloidal metal nanoparticles as a component of designed catalyst. *Physical Chemistry Chemical Physics* **2011**, *13* (7), 2457-2487.

20. Wang, D.; Li, Y., Bimetallic Nanocrystals: Liquid-Phase Synthesis and Catalytic Applications. *Advanced Materials* **2011**, *23* (9), 1044-1060.
21. Zhou, Z.-Y.; Tian, N.; Li, J.-T.; Broadwell, I.; Sun, S.-G., Nanomaterials of high surface energy with exceptional properties in catalysis and energy storage. *Chemical Society Reviews* **2011**, *40* (7), 4167-4185.
22. Gu, J.; Zhang, Y.-W.; Tao, F., Shape control of bimetallic nanocatalysts through well-designed colloidal chemistry approaches. *Chemical Society Reviews* **2012**, *41* (24), 8050-8065.
23. Quan, Z.; Wang, Y.; Fang, J., High-Index Faceted Noble Metal Nanocrystals. *Accounts of Chemical Research* **2012**, *46* (2), 191-202.
24. Sneed, B. T.; Kuo, C.-H.; Brodsky, C. N.; Tsung, C.-K., Iodide-Mediated Control of Rhodium Epitaxial Growth on Well-Defined Noble Metal Nanocrystals: Synthesis, Characterization, and Structure-Dependent Catalytic Properties. *Journal of the American Chemical Society* **2012**, *134* (44), 18417-18426.
25. Wu, J.; Li, P.; Pan, Y.-T.; Warren, S.; Yin, X.; Yang, H., Surface lattice-engineered bimetallic nanoparticles and their catalytic properties. *Chemical Society Reviews* **2012**, *41* (24), 8066-8074.
26. Yu, W.; Porosoff, M. D.; Chen, J. G., Review of Pt-Based Bimetallic Catalysis: From Model Surfaces to Supported Catalysts. *Chemical Reviews* **2012**, *112* (11), 5780-5817.
27. Zhang, H.; Jin, M.; Xia, Y., Noble-Metal Nanocrystals with Concave Surfaces: Synthesis and Applications. *Angewandte Chemie International Edition* **2012**, *51* (31), 7656-7673.
28. Zhou, K.; Li, Y., Catalysis Based on Nanocrystals with Well-Defined Facets. *Angewandte Chemie International Edition* **2012**, *51* (3), 602-613.
29. Kuo, C.-H.; Lamontagne, L. K.; Brodsky, C. N.; Chou, L.-Y.; Zhuang, J.; Sneed, B. T.; Sheehan, M.

- K.; Tsung, C.-K., The Effect of Lattice Strain on the Catalytic Properties of Pd Nanocrystals. *ChemSusChem* **2013**, *6* (10), 1993-2000.
30. Caruso, F., Nanoengineering of Particle Surfaces. *Advanced Materials* **2001**, *13* (1), 11-22.
31. Teng, X.; Black, D.; Watkins, N. J.; Gao, Y.; Yang, H., Platinum-Maghemite Core-Shell Nanoparticles Using a Sequential Synthesis. *Nano Letters* **2003**, *3* (2), 261-264.
32. Lin, K. J.; Chen, L. J.; Prasad, M. R.; Cheng, C. Y., Core-Shell Synthesis of a Novel, Spherical, Mesoporous Silica/Platinum Nanocomposite: Pt/PVP@MCM-41. *Advanced Materials* **2004**, *16* (20), 1845-1849.
33. Sun, X.; Li, Y., Colloidal Carbon Spheres and Their Core/Shell Structures with Noble-Metal Nanoparticles. *Angewandte Chemie International Edition* **2004**, *43* (5), 597-601.
34. Lu, A.-H.; Li, W.-C.; Matoussevitch, N.; Spliethoff, B.; Bonnemann, H.; Schuth, F., Highly stable carbon-protected cobalt nanoparticles and graphite shells. *Chemical Communications* **2005**, (1), 98-100.
35. Sastry, M.; Swami, A.; Mandal, S.; Selvakannan, P. R., New approaches to the synthesis of anisotropic, core-shell and hollow metal nanostructures. *Journal of Materials Chemistry* **2005**, *15* (31), 3161-3174.
36. Ikeda, S.; Ishino, S.; Harada, T.; Okamoto, N.; Sakata, T.; Mori, H.; Kuwabata, S.; Torimoto, T.; Matsumura, M., Ligand-Free Platinum Nanoparticles Encapsulated in a Hollow Porous Carbon Shell as a Highly Active Heterogeneous Hydrogenation Catalyst. *Angewandte Chemie International Edition* **2006**, *45* (42), 7063-7066.
37. Joo, S. H.; Park, J. Y.; Tsung, C.-K.; Yamada, Y.; Yang, P.; Somorjai, G. A., Thermally stable Pt/mesoporous silica core-shell nanocatalysts for high-temperature reactions. *Nature Materials*

- 2009, 8 (2), 126-131.
38. Reiss, P.; Protière, M.; Li, L., Core/Shell Semiconductor Nanocrystals. *Small* **2009**, 5 (2), 154-168.
39. Guerrero-Martínez, A.; Pérez-Juste, J.; Liz-Marzán, L. M., Recent Progress on Silica Coating of Nanoparticles and Related Nanomaterials. *Advanced Materials* **2010**, 22 (11), 1182-1195.
40. Li, J. F.; Huang, Y. F.; Ding, Y.; Yang, Z. L.; Li, S. B.; Zhou, X. S.; Fan, F. R.; Zhang, W.; Zhou, Z. Y.; WuDe, Y.; Ren, B.; Wang, Z. L.; Tian, Z. Q., Shell-isolated nanoparticle-enhanced Raman spectroscopy. *Nature* **2010**, 464 (7287), 392-395.
41. Scharl, W., Current directions in core-shell nanoparticle design. *Nanoscale* **2010**, 2 (6), 829-843.
42. Wu, X.-J.; Xu, D., Soft Template Synthesis of Yolk/Silica Shell particles. *Advanced Materials* **2010**, 22 (13), 1516-1520.
43. Ghosh Chaudhuri, R.; Paria, S., Core/Shell Nanoparticles: Classes, Properties, Synthesis Mechanisms, Characterization, and Applications. *Chemical Reviews* **2011**, 112 (4), 2373-2433.
44. Liu, J.; Qiao, S. Z.; Chen, J. S.; Lou, X. W.; Xing, X.; Lu, G. Q., Yolk/shell nanoparticles: new platforms for nanoreactors, drug delivery and lithium-ion batteries. *Chemical Communications* **2011**, 47 (47), 12578-12591.
45. Wei, S.; Wang, Q.; Zhu, J.; Sun, L.; Lin, H.; Guo, Z., Multifunctional composite core-shell nanoparticles. *Nanoscale* **2011**, 3 (11), 4474-4502.
46. Zhang, Q.; Lee, I.; Joo, J. B.; Zaera, F.; Yin, Y., Core-Shell Nanostructured Catalysts. *Accounts of Chemical Research* **2012**, 46 (8), 1816-1824.
47. Wang, H.; Chen, L.; Feng, Y.; Chen, H., Exploiting Core-Shell Synergy for Nanosynthesis and Mechanistic Investigation. *Accounts of Chemical Research* **2013**, 46 (7), 1636-1646.
48. Chen, Z.; Cui, Z.-M.; Niu, F.; Jiang, L.; Song, W.-G., Pd nanoparticles in silica hollow spheres

- with mesoporous walls: a nanoreactor with extremely high activity. *Chemical Communications* **2010**, *46* (35), 6524-6526.
49. Liu, S.; Han, M.-Y., Silica-Coated Metal Nanoparticles. *Chemistry – An Asian Journal* **2010**, *5* (1), 36-45.
50. Park, J.; Song, H., Metal@Silica yolk-shell nanostructures as versatile bifunctional nanocatalysts. *Nano Research* **2011**, *4* (1), 33-49.
51. Lee, J.; Kim, J.; Hyeon, T., Recent Progress in the Synthesis of Porous Carbon Materials. *Advanced Materials* **2006**, *18* (16), 2073-2094.
52. Suh, W. H.; Jang, A. R.; Suh, Y. H.; Suslick, K. S., Porous, Hollow, and Ball-in-Ball Metal Oxide Microspheres: Preparation, Endocytosis, and Cytotoxicity. *Advanced Materials* **2006**, *18* (14), 1832-1837.
53. Zheng, N.; Stucky, G. D., A General Synthetic Strategy for Oxide-Supported Metal Nanoparticle Catalysts. *Journal of the American Chemical Society* **2006**, *128* (44), 14278-14280.
54. Zhang, Q.; Lee, I.; Ge, J.; Zaera, F.; Yin, Y., Surface-Protected Etching of Mesoporous Oxide Shells for the Stabilization of Metal Nanocatalysts. *Advanced Functional Materials* **2010**, *20* (14), 2201-2214.
55. Mitsudome, T.; Mikami, Y.; Matoba, M.; Mizugaki, T.; Jitsukawa, K.; Kaneda, K., Design of a Silver–Cerium Dioxide Core–Shell Nanocomposite Catalyst for Chemoselective Reduction Reactions. *Angewandte Chemie International Edition* **2012**, *51* (1), 136-139.
56. Sun, H.; He, J.; Wang, J.; Zhang, S.-Y.; Liu, C.; Sritharan, T.; Mhaisalkar, S.; Han, M.-Y.; Wang, D.; Chen, H., Investigating the Multiple Roles of Polyvinylpyrrolidone for a General Methodology of Oxide Encapsulation. *Journal of the American Chemical Society* **2013**, *135* (24), 9099-9110.

57. Li, J.; Zeng, H. C., Size Tuning, Functionalization, and Reactivation of Au in TiO<sub>2</sub> Nanoreactors. *Angewandte Chemie International Edition* **2005**, *44* (28), 4342-4345.
58. Wang, X.; Li, G.; Chen, T.; Yang, M.; Zhang, Z.; Wu, T.; Chen, H., Polymer-Encapsulated Gold-Nanoparticle Dimers: Facile Preparation and Catalytical Application in Guided Growth of Dimeric ZnO-Nanowires. *Nano Letters* **2008**, *8* (9), 2643-2647.
59. Liu, R.; Mahurin, S. M.; Li, C.; Unocic, R. R.; Idrobo, J. C.; Gao, H.; Pennycook, S. J.; Dai, S., Dopamine as a Carbon Source: The Controlled Synthesis of Hollow Carbon Spheres and Yolk-Structured Carbon Nanocomposites. *Angewandte Chemie International Edition* **2011**, *50* (30), 6799-6802.
60. Barakat, T.; Rooke, J. C.; Tidahy, H. L.; Hosseini, M.; Cousin, R.; Lamonier, J.-F.; Giraudon, J.-M.; De Weireld, G.; Su, B.-L.; Siffert, S., Noble-Metal-Based Catalysts Supported on Zeolites and Macro-Mesoporous Metal Oxide Supports for the Total Oxidation of Volatile Organic Compounds. *ChemSusChem* **2011**, *4* (10), 1420-1430.
61. Chen, C.; Fang, X.; Wu, B.; Huang, L.; Zheng, N., A Multi-Yolk-Shell Structured Nanocatalyst Containing Sub-10 nm Pd Nanoparticles in Porous CeO<sub>2</sub>. *ChemCatChem* **2012**, *4* (10), 1578-1586.
62. Chen, G.; Zhao, Y.; Fu, G.; Duchesne, P. N.; Gu, L.; Zheng, Y.; Weng, X.; Chen, M.; Zhang, P.; Pao, C.-W.; Lee, J.-F.; Zheng, N., Interfacial Effects in Iron-Nickel Hydroxide-Platinum Nanoparticles Enhance Catalytic Oxidation. *Science* **2014**, *344* (6183), 495-499.
63. Li, H.; Eddaoudi, M.; O'Keeffe, M.; Yaghi, O. M., Design and synthesis of an exceptionally stable and highly porous metal-organic framework. *Nature* **1999**, *402* (6759), 276-279.
64. Eddaoudi, M.; Moler, D. B.; Li, H.; Chen, B.; Reineke, T. M.; O'Keeffe, M.; Yaghi, O. M., Modular Chemistry: Secondary Building Units as a Basis for the Design of Highly Porous and

- Robust Metal–Organic Carboxylate Frameworks. *Accounts of Chemical Research* **2001**, *34* (4), 319-330.
65. James, S. L., Metal-organic frameworks. *Chemical Society Reviews* **2003**, *32* (5), 276-288.
66. Millward, A. R.; Yaghi, O. M., Metal–Organic Frameworks with Exceptionally High Capacity for Storage of Carbon Dioxide at Room Temperature. *Journal of the American Chemical Society* **2005**, *127* (51), 17998-17999.
67. Sanchez, C.; Julian, B.; Belleville, P.; Popall, M., Applications of hybrid organic-inorganic nanocomposites. *Journal of Materials Chemistry* **2005**, *15* (35-36), 3559-3592.
68. Mueller, U.; Schubert, M.; Teich, F.; Puetter, H.; Schierle-Arndt, K.; Pastre, J., Metal-organic frameworks-prospective industrial applications. *Journal of Materials Chemistry* **2006**, *16* (7), 626-636.
69. Farrusseng, D.; Aguado, S.; Pinel, C., Metal–Organic Frameworks: Opportunities for Catalysis. *Angewandte Chemie International Edition* **2009**, *48* (41), 7502-7513.
70. Koh, K.; Wong-Foy, A. G.; Matzger, A. J., MOF@MOF: microporous core-shell architectures. *Chemical Communications* **2009**, (41), 6162-6164.
71. Lee, J.; Farha, O. K.; Roberts, J.; Scheidt, K. A.; Nguyen, S. T.; Hupp, J. T., Metal-organic framework materials as catalysts. *Chemical Society Reviews* **2009**, *38* (5), 1450-1459.
72. Li, Q.; Zhang, W.; Miljanić, O. Š.; Sue, C.-H.; Zhao, Y.-L.; Liu, L.; Knobler, C. B.; Stoddart, J. F.; Yaghi, O. M., Docking in Metal-Organic Frameworks. *Science* **2009**, *325* (5942), 855-859.
73. Murray, L. J.; Dinca, M.; Long, J. R., Hydrogen storage in metal-organic frameworks. *Chemical Society Reviews* **2009**, *38* (5), 1294-1314.
74. Cohen, S. M., Modifying MOFs: new chemistry, new materials. *Chemical Science* **2010**, *1* (1),

- 32-36.
75. Corma, A.; García, H.; Llabrés i Xamena, F. X., Engineering Metal Organic Frameworks for Heterogeneous Catalysis. *Chemical Reviews* **2010**, *110* (8), 4606-4655.
76. Li, Y.-S.; Bux, H.; Feldhoff, A.; Li, G.-L.; Yang, W.-S.; Caro, J., Controllable Synthesis of Metal–Organic Frameworks: From MOF Nanorods to Oriented MOF Membranes. *Advanced Materials* **2010**, *22* (30), 3322-3326.
77. Bétard, A.; Fischer, R. A., Metal–Organic Framework Thin Films: From Fundamentals to Applications. *Chemical Reviews* **2011**, *112* (2), 1055-1083.
78. Cohen, S. M., Postsynthetic Methods for the Functionalization of Metal–Organic Frameworks. *Chemical Reviews* **2011**, *112* (2), 970-1000.
79. Meek, S. T.; Greathouse, J. A.; Allendorf, M. D., Metal-Organic Frameworks: A Rapidly Growing Class of Versatile Nanoporous Materials. *Advanced Materials* **2011**, *23* (2), 249-267.
80. Shekhah, O.; Liu, J.; Fischer, R. A.; Woll, C., MOF thin films: existing and future applications. *Chemical Society Reviews* **2011**, *40* (2), 1081-1106.
81. Stock, N.; Biswas, S., Synthesis of Metal-Organic Frameworks (MOFs): Routes to Various MOF Topologies, Morphologies, and Composites. *Chemical Reviews* **2011**, *112* (2), 933-969.
82. Almeida Paz, F. A.; Klinowski, J.; Vilela, S. M. F.; Tome, J. P. C.; Cavaleiro, J. A. S.; Rocha, J., Ligand design for functional metal-organic frameworks. *Chemical Society Reviews* **2012**, *41* (3), 1088-1110.
83. Flugel, E. A.; Ranft, A.; Haase, F.; Lotsch, B. V., Synthetic routes toward MOF nanomorphologies. *Journal of Materials Chemistry* **2012**, *22* (20), 10119-10133.
84. Xuan, W.; Zhu, C.; Liu, Y.; Cui, Y., Mesoporous metal-organic framework materials. *Chemical*

- Society Reviews* **2012**, *41* (5), 1677-1695.
85. Zhou, H.-C.; Long, J. R.; Yaghi, O. M., Introduction to Metal–Organic Frameworks. *Chemical Reviews* **2012**, *112* (2), 673-674.
86. Furukawa, H.; Cordova, K. E.; O’Keeffe, M.; Yaghi, O. M., The Chemistry and Applications of Metal-Organic Frameworks. *Science* **2013**, *341* (6149).
87. Gascon, J.; Corma, A.; Kapteijn, F.; Llabrés i Xamena, F. X., Metal Organic Framework Catalysis: Quo vadis? *ACS Catalysis* **2013**, *4* (2), 361-378.
88. Li, S.-L.; Xu, Q., Metal-organic frameworks as platforms for clean energy. *Energy & Environmental Science* **2013**, *6* (6), 1656-1683.
89. Mondloch, J. E.; Karagiari, O.; Farha, O. K.; Hupp, J. T., Activation of metal-organic framework materials. *CrystEngComm* **2013**, *15* (45), 9258-9264.
90. Carné-Sánchez, A.; Imaz, I.; Stylianou, K. C.; Maspoch, D., Metal–Organic Frameworks: From Molecules/Metal Ions to Crystals to Superstructures. *Chemistry – A European Journal* **2014**, *20* (18), 5192-5201.
91. Zhu, Q. L.; Xu, Q., Metal-organic framework composites. *Chem Soc Rev* **2014**, *43* (16), 5468-512.
92. Britt, D.; Furukawa, H.; Wang, B.; Glover, T. G.; Yaghi, O. M., Highly efficient separation of carbon dioxide by a metal-organic framework replete with open metal sites. *Proceedings of the National Academy of Sciences* **2009**, *106* (49), 20637-20640.
93. Li, J.-R.; Kuppler, R. J.; Zhou, H.-C., Selective gas adsorption and separation in metal-organic frameworks. *Chemical Society Reviews* **2009**, *38* (5), 1477-1504.
94. Jiang, H.-L.; Tatsu, Y.; Lu, Z.-H.; Xu, Q., Non-, Micro-, and Mesoporous Metal–Organic Framework Isomers: Reversible Transformation, Fluorescence Sensing, and Large Molecule

- Separation. *Journal of the American Chemical Society* **2010**, *132* (16), 5586-5587.
95. Zou, R.; Abdel-Fattah, A. I.; Xu, H.; Zhao, Y.; Hickmott, D. D., Storage and separation applications of nanoporous metal-organic frameworks. *CrystEngComm* **2010**, *12* (5), 1337-1353.
96. Achmann, S.; Hagen, G.; Kita, J.; Malkowsky, I.; Kiener, C.; Moos, R., Metal-Organic Frameworks for Sensing Applications in the Gas Phase. *Sensors* **2009**, *9* (3), 1574-1589.
97. Kreno, L. E.; Hupp, J. T.; Van Duyne, R. P., Metal–Organic Framework Thin Film for Enhanced Localized Surface Plasmon Resonance Gas Sensing. *Analytical Chemistry* **2010**, *82* (19), 8042-8046.
98. Lu, Z.-Z.; Zhang, R.; Li, Y.-Z.; Guo, Z.-J.; Zheng, H.-G., Solvatochromic Behavior of a Nanotubular Metal–Organic Framework for Sensing Small Molecules. *Journal of the American Chemical Society* **2011**, *133* (12), 4172-4174.
99. Huxford, R. C.; Della Rocca, J.; Lin, W., Metal–organic frameworks as potential drug carriers. *Current Opinion in Chemical Biology* **2010**, *14* (2), 262-268.
100. Xing, L.; Zheng, H.; Cao, Y.; Che, S., Coordination Polymer Coated Mesoporous Silica Nanoparticles for pH-Responsive Drug Release. *Advanced Materials* **2012**, *24* (48), 6433-6437.
101. Zhuang, J.; Kuo, C. H.; Chou, L. Y.; Liu, D. Y.; Weerapana, E.; Tsung, C. K., Optimized metal-organic-framework nanospheres for drug delivery: evaluation of small-molecule encapsulation. *ACS Nano* **2014**, *8* (3), 2812-9.
102. Dhakshinamoorthy, A.; Alvaro, M.; Garcia, H., Commercial metal-organic frameworks as heterogeneous catalysts. *Chemical Communications* **2012**, *48* (92), 11275-11288.
103. Shieh, F.-K.; Wang, S.-C.; Yen, C.-I.; Wu, C.-C.; Dutta, S.; Chou, L.-Y.; Morabito, J. V.; Hu, P.; Hsu, M.-H.; Wu, K. C. W.; Tsung, C.-K., Imparting Functionality to Biocatalysts via

- Embedding Enzymes into Nanoporous Materials by a de Novo Approach: Size-Selective Sheltering of Catalase in Metal–Organic Framework Microcrystals. *Journal of the American Chemical Society* **2015**.
104. Meilikhov, M.; Yusenko, K.; Esken, D.; Turner, S.; Van Tendeloo, G.; Fischer, R. A., Metals@MOFs – Loading MOFs with Metal Nanoparticles for Hybrid Functions. *European Journal of Inorganic Chemistry* **2010**, *2010* (24), 3701-3714.
105. Xiang, Z.; Hu, Z.; Cao, D.; Yang, W.; Lu, J.; Han, B.; Wang, W., Metal–Organic Frameworks with Incorporated Carbon Nanotubes: Improving Carbon Dioxide and Methane Storage Capacities by Lithium Doping. *Angewandte Chemie International Edition* **2011**, *50* (2), 491-494.
106. Dhakshinamoorthy, A.; Garcia, H., Catalysis by metal nanoparticles embedded on metal-organic frameworks. *Chemical Society Reviews* **2012**, *41* (15), 5262-5284.
107. Juan-Alcaniz, J.; Gascon, J.; Kapteijn, F., Metal-organic frameworks as scaffolds for the encapsulation of active species: state of the art and future perspectives. *Journal of Materials Chemistry* **2012**, *22* (20), 10102-10118.
108. Liu, Y.; Tang, Z., Multifunctional Nanoparticle@MOF Core–Shell Nanostructures. *Advanced Materials* **2013**, *25* (40), 5819-5825.
109. Moon, H. R.; Lim, D.-W.; Suh, M. P., Fabrication of metal nanoparticles in metal-organic frameworks. *Chemical Society Reviews* **2013**, *42* (4), 1807-1824.
110. Ricco, R.; Malfatti, L.; Takahashi, M.; Hill, A. J.; Falcaro, P., Applications of magnetic metal-organic framework composites. *Journal of Materials Chemistry A* **2013**, *1* (42), 13033-13045.
111. Hu, P.; Morabito, J. V.; Tsung, C.-K., Core–Shell Catalysts of Metal Nanoparticle Core and

- Metal–Organic Framework Shell. *ACS Catalysis* **2014**, *4* (12), 4409-4419.
112. Aijaz, A.; Xu, Q., Catalysis with Metal Nanoparticles Immobilized within the Pores of Metal–Organic Frameworks. *The Journal of Physical Chemistry Letters* **2014**, *5* (8), 1400-1411.
113. Kuo, C.-H.; Tang, Y.; Chou, L.-Y.; Sneed, B. T.; Brodsky, C. N.; Zhao, Z.; Tsung, C.-K., Yolk–Shell Nanocrystal@ZIF-8 Nanostructures for Gas-Phase Heterogeneous Catalysis with Selectivity Control. *Journal of the American Chemical Society* **2012**, *134* (35), 14345-14348.
114. Li, G.; Kobayashi, H.; Taylor, J. M.; Ikeda, R.; Kubota, Y.; Kato, K.; Takata, M.; Yamamoto, T.; Toh, S.; Matsumura, S.; Kitagawa, H., Hydrogen storage in Pd nanocrystals covered with a metal-organic framework. *Nat Mater* **2014**, *13* (8), 802-6.
115. Zhao, M.; Deng, K.; He, L.; Liu, Y.; Li, G.; Zhao, H.; Tang, Z., Core–Shell Palladium Nanoparticle@Metal–Organic Frameworks as Multifunctional Catalysts for Cascade Reactions. *Journal of the American Chemical Society* **2014**, *136* (5), 1738-1741.
116. He, L.; Liu, Y.; Liu, J.; Xiong, Y.; Zheng, J.; Liu, Y.; Tang, Z., Core–Shell Noble-Metal@Metal-Organic-Framework Nanoparticles with Highly Selective Sensing Property. *Angewandte Chemie International Edition* **2013**, *52* (13), 3741-3745.
117. Hermes, S.; Schröter, M.-K.; Schmid, R.; Khodeir, L.; Muhler, M.; Tissler, A.; Fischer, R. W.; Fischer, R. A., Metal@MOF: Loading of Highly Porous Coordination Polymers Host Lattices by Metal Organic Chemical Vapor Deposition. *Angewandte Chemie International Edition* **2005**, *44* (38), 6237-6241.
118. Muller, M.; Lebedev, O. I.; Fischer, R. A., Gas-phase loading of [Zn<sub>4</sub>O(bt<sub>2</sub>)<sub>2</sub>] (MOF-177) with organometallic CVD-precursors: inclusion compounds of the type [LnM]<sub>a</sub>@MOF-177 and the formation of Cu and Pd nanoparticles inside MOF-177. *Journal of Materials Chemistry* **2008**,

- 18 (43), 5274-5281.
119. Schröder, F.; Esken, D.; Cokoja, M.; van den Berg, M. W. E.; Lebedev, O. I.; Van Tendeloo, G.; Walaszek, B.; Buntkowsky, G.; Limbach, H.-H.; Chaudret, B.; Fischer, R. A., Ruthenium Nanoparticles inside Porous [Zn<sub>4</sub>O(bdc)<sub>3</sub>] by Hydrogenolysis of Adsorbed [Ru(cod)(cot)]: A Solid-State Reference System for Surfactant-Stabilized Ruthenium Colloids. *Journal of the American Chemical Society* **2008**, *130* (19), 6119-6130.
120. Esken, D.; Zhang, X.; Lebedev, O. I.; Schroder, F.; Fischer, R. A., Pd@MOF-5: limitations of gas-phase infiltration and solution impregnation of [Zn<sub>4</sub>O(bdc)<sub>3</sub>] (MOF-5) with metal-organic palladium precursors for loading with Pd nanoparticles. *Journal of Materials Chemistry* **2009**, *19* (9), 1314-1319.
121. Schröder, F.; Henke, S.; Zhang, X.; Fischer, R. A., Simultaneous Gas-Phase Loading of MOF-5 with Two Metal Precursors: towards Bimetallics@MOF. *European Journal of Inorganic Chemistry* **2009**, *2009* (21), 3131-3140.
122. Esken, D.; Turner, S.; Lebedev, O. I.; Van Tendeloo, G.; Fischer, R. A., Au@ZIFs: Stabilization and Encapsulation of Cavity-Size Matching Gold Clusters inside Functionalized Zeolite Imidazolate Frameworks, ZIFs. *Chemistry of Materials* **2010**, *22* (23), 6393-6401.
123. Gu, X.; Lu, Z.-H.; Jiang, H.-L.; Akita, T.; Xu, Q., Synergistic Catalysis of Metal–Organic Framework-Immobilized Au–Pd Nanoparticles in Dehydrogenation of Formic Acid for Chemical Hydrogen Storage. *Journal of the American Chemical Society* **2011**, *133* (31), 11822-11825.
124. Jiang, H.-L.; Akita, T.; Ishida, T.; Haruta, M.; Xu, Q., Synergistic Catalysis of Au@Ag Core–Shell Nanoparticles Stabilized on Metal–Organic Framework. *Journal of the American Chemical Society* **2011**, *133* (5), 1304-1306.

125. Jiang, H.-L.; Lin, Q.-P.; Akita, T.; Liu, B.; Ohashi, H.; Oji, H.; Honma, T.; Takei, T.; Haruta, M.; Xu, Q., Ultrafine Gold Clusters Incorporated into a Metal–Organic Framework. *Chemistry – A European Journal* **2011**, *17* (1), 78-81.
126. Aijaz, A.; Karkamkar, A.; Choi, Y. J.; Tsumori, N.; Rönnebro, E.; Autrey, T.; Shioyama, H.; Xu, Q., Immobilizing Highly Catalytically Active Pt Nanoparticles inside the Pores of Metal–Organic Framework: A Double Solvents Approach. *Journal of the American Chemical Society* **2012**, *134* (34), 13926-13929.
127. Zhu, Q.-L.; Li, J.; Xu, Q., Immobilizing Metal Nanoparticles to Metal–Organic Frameworks with Size and Location Control for Optimizing Catalytic Performance. *Journal of the American Chemical Society* **2013**, *135* (28), 10210-10213.
128. Sugikawa, K.; Furukawa, Y.; Sada, K., SERS-Active Metal–Organic Frameworks Embedding Gold Nanorods. *Chemistry of Materials* **2011**, *23* (13), 3132-3134.
129. Sugikawa, K.; Nagata, S.; Furukawa, Y.; Kokado, K.; Sada, K., Stable and Functional Gold Nanorod Composites with a Metal–Organic Framework Crystalline Shell. *Chemistry of Materials* **2013**, *25* (13), 2565-2570.
130. Lu, G.; Li, S.; Guo, Z.; Farha, O. K.; Hauser, B. G.; Qi, X.; Wang, Y.; Wang, X.; Han, S.; Liu, X.; DuChene, J. S.; Zhang, H.; Zhang, Q.; Chen, X.; Ma, J.; Loo, S. C. J.; Wei, W. D.; Yang, Y.; Hupp, J. T.; Huo, F., Imparting functionality to a metal–organic framework material by controlled nanoparticle encapsulation. *Nature Chemistry* **2012**, *4* (4), 310-316.
131. Liu, Y.; Zhang, W.; Li, S.; Cui, C.; Wu, J.; Chen, H.; Huo, F., Designable Yolk–Shell Nanoparticle@MOF Petalous Heterostructures. *Chemistry of Materials* **2013**, *26* (2), 1119-1125.
132. Pan, Y.; Heryadi, D.; Zhou, F.; Zhao, L.; Lestari, G.; Su, H.; Lai, Z., Tuning the crystal

morphology and size of zeolitic imidazolate framework-8 in aqueous solution by surfactants.

*CrystEngComm* **2011**, *13* (23), 6937-6940.

133. Niu, W.; Zhang, L.; Xu, G., Shape-Controlled Synthesis of Single-Crystalline Palladium Nanocrystals. *ACS Nano* **2010**, *4* (4), 1987-1996.
134. Chang, C.-C.; Wu, H.-L.; Kuo, C.-H.; Huang, M. H., Hydrothermal Synthesis of Monodispersed Octahedral Gold Nanocrystals with Five Different Size Ranges and Their Self-Assembled Structures. *Chemistry of Materials* **2008**, *20* (24), 7570-7574.
135. Dovgolevsky, E.; Haick, H., Direct Observation of the Transition Point Between Quasi-Spherical and Cubic Nanoparticles in a Two-Step Seed-Mediated Growth Method. *Small* **2008**, *4* (11), 2059-2066.
136. Kuhn, J. N.; Tsung, C.-K.; Huang, W.; Somorjai, G. A., Effect of organic capping layers over monodisperse platinum nanoparticles upon activity for ethylene hydrogenation and carbon monoxide oxidation. *Journal of Catalysis* **2009**, *265* (2), 209-215.
137. Li, S.; Shi, W.; Lu, G.; Li, S.; Loo, S. C. J.; Huo, F., Unconventional Nucleation and Oriented Growth of ZIF-8 Crystals on Non-Polar Surface. *Advanced Materials* **2012**, *24* (44), 5954-5958.